

# Synaptic and Cellular Organization of Layer 1 of the Developing Rat Somatosensory Cortex

THÈSE N° 5902 (2013)

PRÉSENTÉE LE 5 NOVEMBRE 2013

À LA FACULTÉ DES SCIENCES DE LA VIE  
LABORATOIRE DE NEUROSCIENCE DES MICROCIRCUITS  
PROGRAMME DOCTORAL EN NEUROSCIENCES

ÉCOLE POLYTECHNIQUE FÉDÉRALE DE LAUSANNE

POUR L'OBTENTION DU GRADE DE DOCTEUR ÈS SCIENCES

PAR

Shruti MURALIDHAR

acceptée sur proposition du jury:

Prof. D. Moore, président du jury  
Prof. H. Markram, directeur de thèse  
Prof. D. Feldmeyer, rapporteur  
Prof. M. Hausser, rapporteur  
Prof. C. Petersen, rapporteur



ÉCOLE POLYTECHNIQUE  
FÉDÉRALE DE LAUSANNE

Suisse  
2013

I'd take the awe of understanding over the awe of ignorance any day.

- Douglas Adams, *The Salmon of Doubt*

## Table of Contents

<b>Acknowledgements.....</b>	<b>1</b>
<b>Résumé .....</b>	<b>1</b>
<b>Abstract.....</b>	<b>3</b>
<b>Chapter 1 Introduction.....</b>	<b>4</b>
Evolution of the Brain .....	4
The Development of the Neocortex.....	5
Layer 1 .....	6
Methods of study .....	8
<i>In vitro methods</i> .....	8
<i>Classification of neocortical cells</i> .....	9
<i>Neural micro-circuitry</i> .....	10
<b>Chapter 2 Materials and Methods.....</b>	<b>12</b>
Slice preparation .....	12
Electrophysiology .....	12
Perforated patch recording.....	14
Morphological reconstructions .....	14
Morphology analyses:.....	14
<i>Subjective morphological analyses</i> .....	14
<i>Objective morphological analyses</i> .....	15
<i>3D Visualisation</i> .....	15
Calcium imaging of L5PC apical dendritic activity .....	16
Single cell transcriptomics.....	16
<b>Chapter 3 Results - Electrophysiology .....</b>	<b>19</b>
Intrinsic electrophysiology properties of single cells .....	19
<i>Five electrophysiological types in L1</i> .....	19
<i>Classical Accommodating Cells (cAC)</i> .....	19
<i>Classical Non-Accommodating Cells (cNAC)</i> .....	19
<i>Bursting Non-Accommodating Cells (bNAC)</i> .....	19
<i>Classical Stuttering Cells (cSTUT)</i> .....	19
<i>Classical Irregular spiking cells (cIR)</i> .....	20

Electrophysiological Circuitry .....	20
<i>Electrical connections</i> .....	20
<i>Synaptic connections</i> .....	21
<b>Chapter 4 Results - Morphology.....</b>	<b>31</b>
Intrinsic morphological properties of single cells .....	31
<i>Expert-based subjective classification</i> .....	31
<i>Neurogliaform Cells with dense axonal arbours (NGC-DA)</i> .....	31
<i>Neurogliaform Cells with Sparse Axonal Arbours (NGC-SA)</i> .....	31
<i>Horizontal Axon Cells (HAC)</i> .....	32
<i>Descending Axon Cells (DAC)</i> .....	32
<i>Large Axon Cells (LAC)</i> .....	32
<i>Small Axon Cells (SAC)</i> .....	32
<i>Rare cell types</i> .....	32
Objective analyses .....	33
<i>Variance analysis</i> .....	33
<i>Feature power analysis</i> .....	33
<i>Principal Component Analysis (PCA)</i> .....	33
<i>Linear Discriminant Analyses (LDA)</i> .....	34
Morphological Circuitry .....	34
<i>Gap junctions</i> .....	34
<i>Synaptic connections</i> .....	34
Morphoelectrical types .....	35
<b>Chapter 5 Discussion and Conclusions .....</b>	<b>50</b>
Single cell properties .....	50
<i>Electrophysiology</i> .....	50
<i>Morphology</i> .....	51
Circuit Properties .....	52
Conclusions.....	53
<b>Appendix .....</b>	<b>54</b>
Single cell transcriptomics.....	54
<i>Results</i> .....	54
<i>Expression patterns in L1</i> .....	57
Cross-layer connectivity .....	58



<i>Results</i> .....	58
<i>L1 and trans-laminar circuits</i> .....	60
Calcium imaging of L5PC dendrites with single cell L1 stimulation .....	61
<i>Results</i> .....	61
<i>Interaction with apical pyramidal dendrites</i> .....	63
<b>References</b> .....	<b>64</b>
<b>Curriculum Vitae</b> .....	<b>70</b>

## Acknowledgements

Considering that it is usually the first and only thing than people will read of this dry technical document, I will try and thank as many people as I possibly can.

I cannot begin without mentioning the ‘original superheros’ of the lab – Thomas Berger for teaching me the trade and my first german swear word; Luca Gambazzi for teaching me the capitals of all the cantons in Switzerland more importantly, to make delicious gnocchi; Michele Pignatelli for helping me keep an utterly cynical view of everything and ofcourse, for giving me his apartment; Rajnish Ranjan for being an excellent teacher, collaborator, trip organiser and the best party organiser ever and ofcourse, Rodrigo Perin, for teaching me the joys of electronics, among other things and for being a fellow nerd/geek

My cohorts – Vincent Delattre, Jean Pierre Ghobril, Monica Favre – for all the complaining sessions, pep talks, beers, coffee times – for being a soldier in arms at the trenches. Onward ho!

Jesper Ryge, Severine Petitprez, Emmanuelle Logette, Costas Anastassiou, Maurizio Pezzoli and Olivier Hagens - for being the heads of reason (or sometimes not!) and excellent guides and friends par excellence

Julie Meystre, Deborah LaMendola, Mimi Herzog and Ying Shi – for your patience, commitment and your madness. It takes a lot to hold down fort in a lab like ours, and you are shining examples

The BBP has been a place where I have interacted with so many people over the years. Felix Schurmann – for letting me sit in a BBP trouble-shooting meeting on my first day. I realized the true value of team spirit in this whole endeavour; Eilif Muller – for untiring encouragement, excellent advice; Martin Telefont – for seemingly endless vats of patience to deal with all the data and for being a voice of reason; Srikanth Ramamswamy – for being a great friend from the very beginning, for all the wonderful discussions and an unfailing never say die attitude

The women behind the whole operation, keeping the chaos in check: Christiane Debono, Catherine Hanriot and Amanda Pingree – for helping me with everything related to administration and most importantly, helping me get to Henry at various times.

Henry Markram for this opportunity, for trusting in a random Indian girl who suddenly emailed him out of the blue, 5 years ago, asking if she could do a PhD in

neuroscience with him. It has been a great pleasure and honour to work with you and I hope I haven't let you down.

The Scheggenburger lab, who so dearly call us the 'Markram Mafia'; the Petersen Lab for being extremely helpful and Steven Gale for the brunches, tai chi classes and for being my classical music buddy.

A big thanks to all the students and faculty of the EDNE Michele Bonnard for holding the program together.

Richard Walker – for being a pillar of sanity and source of excellent food, wine, books and conversation in the middle of all the chaos.

So many of my friends that I have met and spent wonderful times with – Devika Ashok, Kaushik Vaideeshwaran and so many more.

My family – for standing by me through it all and my very best friend,– Abhishek for sticking with me through thick and thin, for the last 10 years.

## Résumé

Dans l'étude présentée ici, nous avons caractérisé systématiquement le circuit, la composition cellulaire et la connectivité synaptique de couche 1 (L1) du cortex somatosensoriel de rats juvéniles (13-16 jours post-natale). Les paramètres électrophysiologiques et morphologiques ont été mesurés en utilisant la technique du patch-clamp suivie d'une coloration histochimique et d'une reconstruction morphologique en 3D. Suivant la convention de classification de Pétilla, nous avons classifié les cellules en fonction de leur type d'activité, et identifié cinq types des cellules par leurs propriétés électro-physiologiques: 'classical Non-Accommodating Cells' (cNAC), 'classical Accommodating Cells' (cAC), 'burst Non-Accommodating Cells' (bNAC), 'classical Stuttering cells' (cSTUT) et 'classical Irregular Spiking cells' (cIR). Une première classification subjective des différents types morphologiques des cellules a identifié les types suivants: 'Neurogliaform Cell with Dense Axon' (NGC-DA), 'Neurogliaform Cell with Sparse Axon' (NGC-SA), 'Horizontal Axon Cell' (HAC), 'Descending Axon Cell' (DAC), 'Large Axon Cell' (LAC) et 'Small Axon cell' (SAC). Une classification objective a affinée et validée la classification initiale à l'aide des méthodes statistiques de l'analyse de la composante principale (PCA) et de l'analyse du discriminant linéaire (LDA).

Nous avons aussi étudié les règles de connectivité entre les cellules de la couche L1. Nos résultats montrent que la majorité des cellules sont connectées via une connexion lente médiée par les récepteurs GABA<sub>B</sub>, comportant parfois une composante GABA<sub>A</sub> rapide. La répétition des stimulations produit une diminution de l'amplitude des potentiels post-synaptiques mesurés, un effet qui n'a pas été observé lors expériences de patch-clamp en mode perforant, mode qui maintient l'intégrité du milieu intracellulaire. Nous proposons que l'atténuation de la réponse mesurée soit causée par la dilution des composants intracellulaires et des messagers secondaires nécessaires à la signalisation des réponses métabotropiques médiées par les récepteurs GABA<sub>B</sub>. La reconstruction morphologique en 3D des paires de cellules connectées a montré la présence de multiples synapses par connexion, avec une moyenne de 9 contacts présumés par connexion détectée par électrophysiologie. La conductance symétrique des jonctions 'gap' était de  $0,054 \pm 0,03$ .

Dans d'autres expériences, nous avons étudié la connectivité inter-laminaire, la modulation de l'activité dans les dendrites apicales par les neurones de la couche L1,

ainsi que les modes d'expression des gènes en L1. Les résultats, bien que non concluants, fournissent des indications utiles pour les futures études.

Mots de clé: neocortex, couche 1, inhibition, interneurones, GABA récepteurs, dendrites apicales, connectivité inter-laminaire, qPCR

## Abstract

In this thesis, we systematically characterised the circuitry, cellular composition and synaptic connectivity of layer 1 (L1) of the somatosensory cortex of juvenile rats (post natal days 13-16). Electrophysiological and morphological parameters were measured using single and multi-cell patch-clamp electrophysiology followed by histochemical staining and 3D morphological reconstruction. Guided by the Petilla convention, we classified cells in term of their firing patterns, identifying five electrophysiological types: classical Non-Accommodating Cells (cNAC), classical Accommodating Cells (cAC), burst Non-Accommodating Cells (bNAC), classical Stuttering cells (cSTUT) and classical Irregular Spiking cells (cIR). We created first a subjective and then an objective classification of different morphological cell types. The subjective classification identified the following types – NGC-DA, NGC-SA, HAC, DAC, LAC and SAC. The initial classification was refined and validated using PCA and LDA.

We also studied connectivity patterns among L1 cells. Our results showed that a majority of the cells were connected by a slow GABA<sub>B</sub> mediated inhibitory connection, with a fast GABA<sub>A</sub> component. Multiple repetitions of stimulation produced a prominent run-down of postsynaptic potential amplitudes, which was not seen in perforated patch-clamp recordings that maintained the intracellular milieu. We propose that the run-down was due to the dilution of intracellular components and depletion of secondary messengers necessary for signalling of postsynaptic metabotropic GABA<sub>B</sub> receptor mediated responses. 3D morphological reconstructions of these pairs of cells, showed the presence of multi-synapse connections with an average of 9 putative contacts per detected electrophysiological connection. The average coupling co-efficient of gap junctions was  $0.054 \pm 0.03$  with symmetrical conductance.

In additional studies, we investigated patterns of inter-laminar connectivity, the modulation of apical dendritic activity by L1 neurons and patterns of gene expression in L1. We hope that the results these studies – single cell electrophysiology, morphology and connectivity analysis - provide useful hints for future studies of neocortical L1.

Key words: neocortex, layer 1, single cell properties, inhibition, interneurons, GABA receptors, apical dendrites, inter laminar connectivity, qPCR.

# Chapter 1 Introduction

This thesis presents a systematic study of Layer 1 (L1) of the somatosensory cortex of juvenile rat (post-natal day 13-16). The study focuses on cell morphology, electrophysiology, and connectivity. In the appendix, we report additional experiments in which we explored the connections of L1 cells to other layers, gene expression patterns, and the influence of layer 1 cells on apical dendritic processing in L5 pyramidal cells.

Cellular morphologies were reconstructed in 3D using Neurolucida and classified into six groups, first using subjective methods and subsequently through an objective classification scheme. Each group contained a roughly equal number of neurons. Measurements of their electrophysiological behaviour and subsequent classification using the Petilla convention identified five types of neurons. The prominent electrophysiological type was cNAC. L1 interneurons, forming circuits, included both synaptic and electrical gap junctions. All synapses were inhibitory. We observed three different kinds of post-synaptic responses mediated by GABA<sub>A</sub>, GABA<sub>B</sub> and GABA<sub>A+B</sub> receptors respectively. The gap junctions were symmetrical with similar conductance in both directions.

Our study of interlayer connectivity showed very low connection probabilities. Gene expression patterns in L1 were mostly similar to other interneurons, except for the presence of certain neuropeptides. We did not observe any measurable effect of L1 cells on dendritic processing by pyramidal cells in L5.

## Evolution of the Brain

All living cells respond to external and internal stimuli and engage in signal processing. In most metazoans, however, a subset of unique somatic cells form an organised constellation of cells (neurons) specialised for the repeated conduction of an excited state to other neurons (Kaas John H, Evolutionary Neuroscience, 2009). This is the nervous system.

According to a hypothesis proposed by Parker in 1919 (The Elementary Nervous System, Parker, 2012), the “neuromuscular system” evolved in three major stages. At first, it consisted only of muscles, which responded directly to environmental stimuli. This 'neuroid' transmission can be considered the forerunner of nervous activity. The second step saw the evolution of a receptor-effector system in which the receptors arose from epithelial cells positioned close to the differentiated muscles cells. In the final stage, a third type of cell, the protoneuron, created connections between the sensory and effector cells forming a true nervous system. One of the first uses of this

‘proto’ nervous system was the detection of changes in ambient light and the chemical environment.

Over time, changes in environment resulted in the rapid adaptation of organisms. Tracing evolution to the nearest common ancestor of the mammals, one of the main changes of the nervous system was the increase in neuron number and complexity of connectivity. This increase resulted in the appearance of dedicated areas for specific function. The neocortex probably arose as a result of such a specialisation in mammalian-like animals in the early Mesozoic era.

## **The Development of the Neocortex**

In development, the embryonic nervous system forms at a relatively late stage, after the formation of the endoderm, mesoderm and ectoderm. The neural plate forms from a sheet of ectodermal cells, guided by gradients of transcription factors. It then involutes to form the neural tube. Helped by polarity molecules (Hox, Shh, BMP and Retinoic acid), the anterior and posterior ends of the neural tube differentiate into the prosencephalon, mesencephalon and the diencephalon. The prosencephalon, develops further to give rise to the telencephalon and eventually the cerebrum and the neocortex.

Lamination in the neocortex involves two zones of proliferation – the marginal zone and ventricular zone. Neurogenesis occurs mainly in the ventricular zone, while the marginal zone splits consecutively to give rise to the subventricular zone, intermediate zone, the subplate and the cortical plate (CP) radiating outward in the direction of the pia (Principles of Neural Science, Kandel et al., 2012). Radial glial cells provide scaffolding for the migration of newly divided precursors in the Ventricular Zone (VZ) and the Sub ventricular zone (SVZ) to reach their destined layer in the cortical plate.

In 1893, Ramon y Cajal and Magnus Gustaf Retzius used Golgi staining to characterize what are now known as Cajal Retzius cells (Cajal, 1995; Meyer et al., 1999). It is now known that these cells secrete an extracellular matrix protein called Reelin that plays a vital role in the formation of the neocortical layers, (Lacor et al., 2000; Meyer and Goffinet, 1998), acting as a dissociation signal for clustered migrating neurons. In the early stages of development, Cajal Retzius cells also contribute to spontaneous activity that helps to regulate the formation of electrophysiologically active cell networks (Aguilo et al., 1999). Studies show that in rats, the axons shrivel up and disappear around postnatal day 11 (P11), causing the cells to gradually lose their characteristic morphology (Hestrin and Armstrong, 1996; Portera-Cailliau et al., 2005) Along with Cajal Retzius cells, L1 is also the first recipient of developing interneurons



originating in and migrating from the ganglionic eminence (Wonders and Anderson, 2006). These interneurons, along with the pyramidal cells make up the entire population of neurons in the neocortex.

One of the most striking features of the neocortex is the cortical column. A cortical column is a tightly interconnected vertical array of neurons driven by a small number of specific inputs (Mountcastle, 1957). For example, in cats and humans, each ocular dominance column receives input from one eye (Swisher et al., 2010) and each column in the rat barrel cortex receives input from a single whisker (Woolsey and Van der Loos, 1970). Within the column, cells in different layers (1 to 6) connect among themselves according to pre-defined rules. This leads to the formation of localised circuits and the compartmentalisation of neural activity. This basic columnar pattern repeats across the whole cortex (Fulton, 1949; Toyama et al., 1974; Peters and Jones, 1985) leading to the self-regulation of local activity, modulation of long range activity, finally resulting in larger-scale changes in downstream signals to peripheral targets.

## **Layer 1**

Layer 1 is mainly made up of long-range fibres and sparse interneurons and is the thinnest of all layers in the neocortex. It is also the least populated layer (Hestrin and Armstrong, 1996).

To date, most L1 studies have focused on the properties of individual cells and on long-range connectivity between L1 cells and other brain areas and regions.

Advances in staining for cellular markers have made it possible to identify a wide variety of other L1 morphologies. However, there is still no consensus on their classification. Using Golgi and Nissl staining, in the developing occipital cortex of rats (P2 to P35) Bradford et al. identified five morphological types of L1 neurons: foetal horizontal cells, persisting horizontal cells, vertical cells, classical non-pyramidal cells and non-axonal cells (Bradford et al., 1977). By contrast, a study of juvenile rats (P0 - P21) by Zhou and Hablitz, identified only four types: Cajal-Retzius cells, Cells with Confined Axons, Cells with Axons not confined to Layer 1 and Vertical Axon Cells (Zhou and Hablitz, 1996). One of the main reasons for this disparity could be the use of different methods. While the first study used Golgi and Nissl staining, the second used single cell biocytin filling. The advantage of the biocytin method is that it makes it possible to quantify subcellular structures such as spines and boutons – additional information that can modify cell classification.

Subsequent landmark studies have matched morphological data against data from single cell electrophysiology. An important first step was the identification of L1

cells as interneurons. In their immunohistological study of cat visual cortex, Gabbott and Somogyi observed that all L1 neurons are positive for the inhibitory neurotransmitter GABA (Gabbott and Somogyi, 1986).

In 1996, a study of the rat somatosensory cortex (P7 to P19) by Hestrin and Armstrong (Hestrin and Armstrong, 1996) measured the electrophysiological properties (spike halfwidth, resting membrane potential input resistances) of three morphological types - Axon Horizontal Cells (AHC), Axon Descending Cells (ADC) and Neurogliaform (Ngf) cells but did not use the results to propose a morpho-electrical classification. A more recent study by Williams et al., (Wozny and Williams, 2011) classified L1 cells from the adult rat somatosensory cortex (P24 - P36) into four morphological types, including Neurogliaform Cells (NGFC), and Cells with Vertical Axons, and four electrophysiological types: Regular Spiking (RS), Fast Spiking (FS), Burst Spiking (BS) and classical Accommodating Cells (cAC). By combining these individual properties, they identified four morpho-electrical groups – cAC and NGFC; cAC and FS; BS, cAC and NGFC and finally, cAC and BS. Another study by Bekkers et al. used transgenic GAD<sub>67</sub>-GFP (Glutamate decarboxylase - 67 – Green Fluorescent Protein) P14-P25 mice to categorize L1 cells in the anterior piriform cortex (Suzuki and Bekkers, 2010a, 2010b), this time finding seven different morpho-electrical classes,

As seen, each of these classification strategies group L1 cells in different ways. There are several reasons for these discrepancies. These include the choice and particularly the age of the model system, the region of the brain under investigation, the definitions of the threshold currents used for electrophysiological classification, and especially, the quality and ‘completeness’ of morphological reconstructions.

Regardless of these issues, new information has led to a resurgence of interest in the functional role of layer 1, which is now believed to play a major role in neocortical information processing. More specifically, L1 has been shown to play a vital role in the modulation of input from subcortical areas and from other areas of the cortex. A large body of work has demonstrated the role of L1 as a major recipient of short and long-range fibres. These fibres projecting to L1 can be categorized as columnar or non-columnar. Columnar fibres are made up of axons from L2/3 interneurons and PCs, L5PCs (Oberlaender et al., 2011) and Martinotti cells (MCs) (Wang et al., 2004). Most non-columnar inputs come from long-range fibres, many of which originate in primary motor cortex and secondary somatosensory cortex (Cauller, 1995). Thalamocortical inputs arrive primarily from the posterior nucleus of the thalamus (Oda et al., 2004; Rubio-Garrido et al., 2009).

Letzkus et al. have recently demonstrated the functional and behavioural significance of these long-range fibres by studying how cholinergic long - range fibres modulate L1 activity in fear responses, and the way basal forebrain stimulation affects cellular firing frequencies in L1. They show that application of NBQX, an AMPA receptor blocker, decreases the baseline, but not the response profile. Nicotinic blockers (MEC and MLA) completely block the control response profiles (Letzkus et al., 2011).

In another *in vivo* study, Palmer et al. show that interhemispheric inhibition is mediated by callosal fibres that modulate the activity of L1 interneurons, indirectly influencing the apical dendritic activity of pyramidal cells (Palmer et al., 2012).

A study by Chu et al. suggests that synaptic connections between L1 cells are mediated by a non-classical form of GABA<sub>A</sub> receptor with slower dynamics than the GABA<sub>A</sub> connections typically found in FS cells (Chu et al., 2003). In general, however, there have been relatively few studies of connectivity between layer 1 cells and other cells in the same layer.

In sum, we lack a comprehensive picture of the morphology and function of the different types of neurons present in L1; of their long-range connectivity or of the way they interact within the layer. The work presented in this thesis attempts to fill this gap by describing their distinct electrophysiological and morphological properties, their cross-layer circuitry and, most importantly, their local connectivity.

## **Methods of study**

### **In vitro methods**

Understanding the design of an individual layer in the neocortex requires precise measurements of single cell electrophysiology, unbiased morphological analyses, the study of gene expression patterns, and the characterisation of local and long-range connectivity and circuits, which are best obtained using *in vitro* methods. The main methodological challenge is to maintain physiological conditions so that the individual neurons are not perturbed and the properties of the circuitry remain as close as possible to biological values

Slices are easier to handle than full brains. However, *in vitro* and *in vivo* studies often yield contrasting results. *In vitro* studies use traumatised tissue in which many connections have been severed. It is hardly surprising, therefore, that they have physiological properties that are very different from those observed *in vivo*. The major

differences between *in vivo* and *in vitro* electrophysiology are elegantly explained in studies by Thomson et al (Thomson and Deuchars, 1997; Thomson et al., 1996), which showed that the probability of connections between pyramidal cells increased threefold when the slice thickness increased from 400 to 500 microns. Given that inhibitory interneurons on and slightly below the surface of the slice are sensitive to ischemia, hypoxia and tissue damage, increasing the thickness of the slice increases the number of healthy interneurons contributing to connectivity.

Observations of circuit behaviour in *in vitro* preparations may also be incomplete or incorrect since slices have no long-range connections. This poses a problem, especially in the neocortex, whose *in vivo* activity is driven by vital modulatory inputs from the thalamus. Given these issues, caution is required when hypothesizing *in vivo* function from *in vitro* data.

Nonetheless, *in vitro* methods also have many advantages. Slice electrophysiology allows us to study the brain at the cellular and molecular level without having to deal with animal immobilisation and anaesthesia, or with problems related to the depth of penetration of patch pipettes (Steriade, 2001). In particular, they allow experiments requiring precise control over the extracellular ionic environment and the use of glass pipettes and other probes. *In vitro* techniques have made it possible to investigate the actions of neurotransmitters on specific types of neurons, following the blockage of synaptic transmission. Different methods and angles of slicing have contributed to the study of previously inaccessible neuronal types and of spontaneous and evoked rhythmic activities. Single neuron patch clamping in slices has made an enormous contribution to understanding the electrical properties of different neuronal types and their role in the generation of spontaneous electrical activity. The same technique has also made it possible to study the transformation of neuronal signals as a function of membrane potential and voltage and ligand gated conductances. Finally, patch clamping has been extensively used in connectivity studies, elucidating and classifying the structures of local circuits up to 100 to 200  $\mu\text{m}$  in diameter (Perin et al., 2011).

### **Classification of neocortical cells**

One of the key issues in the study of any part of the brain is the classification of its component cells. Early studies made a broad distinction between pyramidal and non-pyramidal cells. However the variety of cell morphologies present in the neocortex was only fully recognized after Camillo Golgi's invention of the Golgi stain in 1873 and

Ramon y Cajal's systematic layer by layer study of human brain samples, using the new method (Peter and Jones, *Cerebral Cortex*, Plenum Press, 1984).

Subsequent work on the classification of cortical cells has used a variety of molecular and electrophysiological methods. The late 1970s saw the first use of specific molecular markers. One of the first results was the discovery that only non-pyramidal cells express Gamma amino decarboxylase (GAD). This made it possible to use GAD as a marker (Ribak, 1978; Ribak et al., 1979). Other markers were subsequently discovered in subpopulations of non-pyramidal cells with distinct morphologies. These include calcium binding proteins such as Calretinin, Calbindin and Parvalbumin and neuropeptides like Vasoactive intestinal peptide (VIP), Cholecystokinin (CCK) and Somatostatin (SST) (Kubota and Kawaguchi, 1994; Kawaguchi, 1995; Kawaguchi and Kubota, 1997; Kawaguchi and Kondo, 2002).

Molecular and morphological classifications were subsequently improved and enriched through the use of single cell patch clamping. The technique, introduced by Neher and Sakmann in 1981 (Neher et al., 1978; Hamill et al., 1991), made it possible to fill individual cells with biocytin and thus to obtain fine-grained reconstructions of neuron morphologies. They also enabled measurements of the electrical properties of individual cells, allowing robust classifications based on their combined electrical and morphological properties.

Further advances in the field have made it possible to measure concentrations of gene transcripts, for populations of single cells, permitting the development of classification techniques that enrich the methods mentioned above with transcriptomics (Cauli et al., 1997). It should be noted, however, that the use of these methods is fraught with technical difficulties - especially when cells are small and fragile - conditions in which it is difficult to obtain all three classes of data, while maintaining high quality.

The ultimate aim of any classification experiment is to obtain clean datasets from different domains that can be combined to give a near complete description and definition of a given cell type. Although much has already been achieved, this is still very definitely a work in progress and many problems remain to be resolved.

### **Neural micro-circuitry**

A second critical issue in any study of the cortex is how to identify the short-range connections between neurons and the local circuits they form. Until the recent introduction of optogenetics (Zemelman et al., 2002; Lima and Miesenböck, 2005), the most effective method available was multipatch clamping.

In 1997, Markram, Lubke and Sakmann used this multipatch clamping to measure subthreshold excitatory PSPs between pyramidal cells in the neocortex of juvenile rats, thus identifying connections between these neurons (Markram et al., 1997). While this initial work used just two electrodes, subsequent developments made it possible to use up to 12 electrodes simultaneously, allowing the identification of repeated connectivity motifs (Perin et al., 2011)

The main limitation of multipatch clamping is the difficulty and cost of constructing and operating setups with large numbers of pipettes. The currently preferred alternative is to use optogenetic techniques. Optogenetics make it possible to stimulate very large numbers of cells. Given however that the new techniques can only detect suprathreshold PSPs, recording subthreshold cellular responses (essential for the detection of connections) still requires patch clamping. In brief, we still do not have the ability to fully characterize the connectivity and activity of local microcircuitry.

## Chapter 2 Materials and Methods

### Slice preparation

Experiments were carried out according to Swiss National and Institutional guidelines. 13 to 16 day old, non-anaesthetised Wistar rats were rapidly decapitated and their brains carefully removed and kept in iced, artificial cerebrospinal fluid (aCSF). 300  $\mu\text{m}$  thick parasagittal slices, approximately 1.7 - 2.2 mm lateral to the midline slices were cut on an HR2 vibratome (Sigmund Elektronik, Heidelberg, Germany) with a 5° incline. The primary somatosensory cortex (SSC) on the slice was located by the anterior extremity of the hippocampus (bend of the CA3 region). Hind limb SSC was designated as  $\pm 1$  mm from this extremity and all cells in L1 were patched within this region. The slices were incubated at 35°C for 30 minutes and left at room temperature in the holding chamber, until recording.

### Electrophysiology

Cells were visualised by Infrared Differential Interference Contrast microscopy (IR-DIC) (Olympus BX51WI microscope, PCO CCD imaging or VX55 Photonics camera) (Stuart et al., 1993). L1 cells were selected according to their positions (not more than 100 microns away from the pia). Cells at the layer 2-3 interface were avoided. Slices kept on the electrophysiological setup were continuously superfused with aCSF containing (in mM) 125 NaCl, 25 NaHCO<sub>3</sub>, 2.5 KCl, 1.25 NaH<sub>2</sub>PO<sub>4</sub>, 2 CaCl<sub>2</sub>, 1 MgCl<sub>2</sub> and 25 D-glucose, bubbled with 95% O<sub>2</sub> – 5% CO<sub>2</sub>. The intracellular pipette solution contained (in mM) 110 Potassium Gluconate, 10 KCl, 4 ATP-Mg, 10 Phosphocreatine, 0.3 GTP, 10 HEPES and 13 Biocytin, adjusted to 290 - 300 mOsm/Lt with D-Mannitol (25 - 35 mM) at pH 7.3.<sup>1</sup> Chemicals were sourced from Sigma Aldrich (Stenheim, Germany) or Merck (Darmstadt, Germany). Gabazine (SR 95331 hydrobromide Ref. no. 1262, Tocris Biosciences) was used at a working concentration of 20  $\mu\text{M}$ , diluted from a 20 mM stock solution and CGP55845 (Tocris Biosciences, Ref. no. 1248) was used at working concentration of 4  $\mu\text{M}$ , diluted from a 10 mM stock made in DMSO. Care was taken to keep the working concentration of DMSO to levels less than 1 in 1000 to avoid any chances of cellular toxicity.

Multiple somatic whole cell recordings (1 - 6 cells) were performed with Axopatch 200B amplifiers in current clamp mode at  $34 \pm 1^\circ\text{C}$  bath temperature. Data acquisition was performed via an ITC-18, connected to a Macintosh, running a custom written routine in

---

<sup>1</sup> The membrane potential values cited have not been adjusted for the liquid junction potential, which was approximately -14 mV

IGOR Pro (Version 6.05A, Wavemetrics, Portland, OR, USA). Voltage signals were sampled at rates between 5 and 10 kHz and filtered with a 2 kHz Bessel filter. Patch pipettes with a tip resistance of 3 - 8 M $\Omega$  were pulled with a Flaming/Brown micropipette puller P-97 (Sutter Instruments and Co.) using borosilicate glass capillaries with filaments (Article code number 1403513, Hilgenberg). Experiments were performed both with standard intracellular solution (as described in Slice Preparation) and with Amphotericin B for normal and perforated patch-clamp, respectively.

Intrinsic electrical properties of the cells were measured using different stimuli and calibrated current intensities. Calibration was performed by varying the amplitude of a square pulse of 50 pA until it elicited a single action potential. The cells were then left undisturbed at native resting membrane potentials. As soon as electrical access was obtained, a predefined set of stimuli (e-code) was applied .

Cells were classified in terms of the basic types defined in the Petilla Interneuron Convention (Ascoli et al., 2008). We identified five electrophysiological neuron types (e-types), each characterised by a specific firing pattern: classical Accommodating Cells (cAC), classical Non-Accommodating Cells (cNAC), bursting Non-Accommodating Cells (bNAC), classical Stuttering Cells (cSTUT) and classical Irregular Spiking Cells (cIR). For each cell, we plotted Inter Spike Intervals (ISIs) against AP sequence order. This gave us a linear regression line and a coefficient of correlation to quantify the goodness of fit to the linear regression. Cells whose regression line had a slope greater than or equal to 1 and whose sum of the Root Mean Square (RMS) error was less than 30 (mean = 28.76), were classified as Accommodating Cells. Cells whose regression line had a slope less than 1 and whose sum of the RMS errors were less than 30 (mean = 20.11), were classified as Non-Accommodating Cells. Cells whose regression lines had RMS errors greater than 30 were separated into cSTUT/cIR group for further analysis. For our final classification, we combined this information with information about the pattern of ISI in the AP train. We also further investigated the properties of cells using other stimuli as listed in **Table 1**

Synaptic connections were measured by applying presynaptic stimuli (a train of action potentials (APs) elicited by current pulses at varying frequencies) plus a “recovery test pulse” (RTR) 500 ms after the train. The pulse duration was 3 ms with amplitude of 1–2 nA. This was usually sufficient to trigger reliable and precisely timed APs. The postsynaptic membrane potential was current clamped to approximately –57 mV in order to increase the electric driving force ( $E_{Cl} = -69$  mV). If a synaptic connection was detected, we iterated the procedure 10 to 20 times with inter-stimulus intervals (ISIs) of 30, 60, 90 and 120 seconds. C.V (Co-efficient of Variation) was calculated by dividing the S.D (Standard Deviation) of the single IPSP amplitudes by the mean value.



Single cell and synaptic parameters were extracted with the help of custom-made scripts in IGOR Pro (Version 6.05A) and Matlab (R2009b). Total amplitude values of the Inhibitory Post Synaptic Potentials (IPSPs) were calculated peak to peak. Rise and decay times of the IPSPs were calculated at 20 - 80% of the total amplitude.

### **Perforated patch recording**

A 240 µg/ml stock solution of Amphotericin B (Sigma-Aldrich – Cat no. A-4888) in Dimethylsulfoxide (DMSO) was prepared. A working concentration of 120 µg/ml was achieved by sonicating 8 µl of stock in 1 ml of Intracellular Solution (ICS). The tip of the pipette was back-filled with normal ICS solution until the end of the taper. This was then layered with approximately 20 µl of Amphotericin-ICS following which; the pipette was quickly fitted on to the silver wire electrode. Care was taken to apply minimum positive pressure and to minimize movement within the tissue before reaching the chosen cells. Once adequate electrical access (access resistance values < 20 MΩ) was achieved, the cell was current clamped and stimulation protocols applied.

### **Morphological reconstructions**

The staining and mounting procedure resulted in shrinkage of the slice to 50 - 75% of its original 300 µm thickness. Reconstructions were corrected for this value. The anisotropic shrinkage along the X - Y plane was around 0 - 10% and not corrected. The cells were reconstructed in 3D under an Olympus BX 51W microscope with a water-immersion 60 (NA 0.9) or an oil-immersion 100X (NA 1.35) objective using Neurolucida software (MicroBrightField, Magdeburg, Germany). Reconstructed neurons and connections were analysed both with NeuroExplorer (MicroBrightField) and custom written scripts in Matlab. The list of parameters extracted closely match those reported in (Wang et al., 2002). Putative synaptic contacts were identified as close appositions of boutons and dendrites in the same focal plane.

### **Morphology analyses:**

#### **Subjective morphological analyses**

Morphological parameters (similar to those listed in (Wang *et al.*, 2004) were extracted using NeuroExplorer and used as the basis for an initial subjective classification of morphological types. **Table IV** lists the main parameters used in the classification and the p-values that are most significant.

## Objective morphological analyses

An objective analysis of the L1 morphologies was performed to validate the initial subjective classification scheme. Principal Component Analysis (PCA) and Linear Discriminant Analysis (LDA) were applied using custom Python code and the Scikit-learn machine learning Python module (Pedregosa, 2011) on the normalised dataset. The central idea of principal component analysis (PCA) is to reduce the dimensionality of a dataset consisting of a large number of inter-related variables, while retaining as much as possible of the variation present in the dataset. The initial uncorrelated principal components (PCs) are transformed and ordered as per the amount of variation retained (Jolliffe, 2002). LDA maximises the ratio of between-class variance to within-class variance, enabling similar elements in the dataset to group together and maximising the distance between dissimilar elements. Following LDA, ten-fold cross-validation was performed to determine the accuracy of the resulting linear classifier. In order to ensure that overfitting was not occurring during LDA, ten rounds of ten-fold cross-validation were performed on the same data set with class assignments randomised. A student's t-test was used to compare the scores from the actual data set to the pooled scores of the randomized data sets.

Additional descriptive morphological features were appended to the original list of parameters to better describe the spatial spread and the branching parameters of the reconstructions (**Table V**).

A first LDA trial was performed with six groups, matching the initial subjective classification. The analysis was then re-run first removing the DAC group and then combining the NGC groups.

## 3D Visualisation

Construction of large-scale 3D models of neural microcircuitry requires specialised applications to position and connect thousands of morphologically complex 3D neurons. The EPFL Blue Brain Project has developed custom software for this purpose. The BlueBuilder application allows a user to define the macroscopic shell and recipe for a neural microcircuit, load and position 3D neuron models within the shell, detect putative appositions between neurons, and ultimately export a circuit configuration file that other applications can use for simulation and visualization. In the work described here, 3D neural circuits were visualised using RTNeuron a multi-threaded multi-GPU (Graphics Processing Unit) application developed by the project (Hernando et al., 2008).

## Calcium imaging of L5PC apical dendritic activity

Para-sagittal neocortical slices were cut from the juvenile rat brain, as described earlier. Experiments and imaging was carried out using the slice likely to have the most intact layer 5 pyramidal cell apical dendrites (the ‘parallel’ slice). L1 cells were chosen under a Dodt contrast gradient (Luigs and Neumann), patched and filled with Alexa – 594 hydrazide (10  $\mu$ M, A10442, Molecular Probes). A Layer 5 Pyramidal Cell (L5PC) directly below the L1 cells was patched and filled with Oregon Green 488 BAPTA-1, hexapotassium salt (O-6806, Molecular Probes) and Alexa-594. The two photon experiments were performed with a femtosecond pulsed infrared excitation light of 880 nm, generated by a MaiTai laser (SpectraPhysics) and focused via a  $40 \times 0.8$  NA water immersion objective (Olympus). An E650SP filter (Chroma Technology) prevented backscattered infrared light from hitting the photomultiplier tubes (PMTs). A dichroic mirror followed by band-pass filters split emitted fluorescence into a red ( $607 \pm 22.5$  nm) PMT channel and a green ( $525 \pm 35$  nm) PMT channel. The green channel was used to visualise GFP and the red channel was used to visualise the patch-clamp pipette and the L1 neuron (Gentet et al., 2010). The L5PC was left to fill for up to one hour. The stimulation protocol and line scanning began as soon as the apical branches were clearly visible.

L1 cells were stimulated with a series of pulses, testing the effect on the back propagating calcium-mediated AP in the apical dendrites of the L5PC. Pulses of 3 spikes at 20, 40, 50 and 70 Hz were applied to individual L1 cells, 1.5, 1.5 and 0.5 s before and after L5PC stimulation (**Fig 20b**). The line scan had an acquisition time of 5 seconds, the line width varied according to the chosen scan area. The value of the line period was between 2.5 to 3 s. Linescans were processed in ImageJ (1.45n). The final analyses were performed in Matlab (R2009b).

## Single cell transcriptomics

To study mRNA expression patterns, we performed cytoplasm aspirations from single neurons in L1. Protocols were developed by Monyer and Jonas, and are described in detail as follows, (Single Channel Recording, Sakmann and Neher, Springer Press 2009). Slices were made following the same protocol as for routine electrophysiology. The setup, holders and silver wire electrodes were wiped with RNaseZAP (R2020, Sigma Aldrich). Borosilicate glass pipettes were baked in a dry heat oven at 200 °C for 4 hours. The ICS was made with RNase - free water, filtered (0.2 $\mu$ m pore filter, Millipore Cat no. SLGV033RS) and autoclaved prior to aliquoting. The original recipe was modified to exclude ATP-Mg, phosphocreatinine and GTP, since these components are extremely heat

labile. Pipettes were pulled to have a tip resistance up to 2.5 MΩ and filled with 4 to 6 μl of ICS. L1 neurons were targeted and patched as in a normal electrophysiology experiment and a standard set of stimuli was applied. On completion of the electrical protocols, gentle and sustained negative pressure (50 to 200 mbar) was applied for a short period of time (3 minutes) to aspirate the contents of the cell into the glass pipette. The pressure was maintained for three minutes and/or until the soma visibly shrank. The pipette was then slowly withdrawn, passed repeatedly through the air liquid interface to remove any extracellular debris on the outside walls, and mounted on the holder of a custom-built frame. Using the frame, the pipette was slowly lowered into a 200 μl PCR tube filled with 1 μl of RNase Inhibitor (40 units/μl). The tip of the glass pipette was broken by gently pushing it against the bottom of the tube. Once a faint crack was felt, the pipette was elevated and the contents expelled applying weak positive pressure. All samples were stored at -80°C and tested against three controls. RNase free water provided a negative control for the PCR procedure. A second ICS control tested for solution contamination. To test for the presence of extraneous extracellular material, a pipette was filled with ICS and left for 2 to 3 minutes, close to the position of an aspirated cell. The content of the pipette provided a third tissue/slice control.

We used a high capacity RNA to cDNA kit (Catalog number 4387406, Invitrogen) to convert the single cell mRNA to cDNA. Specific genes (see Taqman assay list) were pre-amplified using the Taqman PreAmp Master Mix (Catalog number 4391128, Invitrogen). Hamilton liquid handling system was used to fill a 384 well plate with three samples for each gene for each aspirated cell. Quantitative PCR (qPCR) was performed using the Applied Biosystem 7900HT Fast Real-Time PCR System and gene specific Taqman assays (see Taqman assay list). Efficiencies of these assays were calculated using the 'Ct slope method' and a series of ten-fold template dilutions. The threshold cycle or Ct was plotted against the log of known cDNA concentrations.. The results of the qPCRs for each of the tested genes was normalised to the expression levels of β-actin using the following equation from Zucker et al., (Zucker et al., 2005):

$$V = (1 + E_{reference})^{Ct(reference)} / (1 + E_{target})^{Ct(target)}$$

where,

V = relative value of the target gene normalised to the reference gene (in this case, β-actin)

E = primer efficiency

Ct = threshold crossing cycle number

Both the Ct-values and the V-values were taken into account for studying changes in target gene expression levels.

**Taqman assay list :**

S.no	Gene name	Taqman assay id
1	Beta-Actin	Rn00667869_m1
2	Calbindin (CB)	Rn00583140_m1
3	Calretinin (CR)	Rn00588816_m1
4	Parvalbumin (PV)	Rn00574541_m1
5	GAD65	Rn00561244_m1
6	GAD67	Rn00566593_m1
7	Neuropeptide Y (NPY)	Rn01410145_m1
8	Pro opiomelanocortin (POMC)	Rn01473378_m1
9	Reelin	Rn00589609_m1

## **Chapter 3 Results - Electrophysiology**

### **Intrinsic electrophysiology properties of single cells**

#### **Five electrophysiological types in L1**

Compared to cortical pyramidal cells, L1 cells are harder to maintain in an electrophysiologically viable state for long periods of time - partly due to their small size (Zhou and Hablitz, 1996). Small cells are also more vulnerable to physical damage (shrinkage and/or swelling) and loss of gigohm seals. For our study, we were nonetheless able to select 98 cells out of 810 with AP amplitudes greater than 50 mV and access resistances less than 10 M $\Omega$ .

#### **Classical Accommodating Cells (cAC)**

Accommodating Cells, which begin to spike with the onset of stimulus, which do not produce bursts and which do not display a delayed response, were classified as classical Accommodating Cells (cAC) (**Fig 1a-a**). 10% of the L1 cells in our sample (n = 11) belonged to this e-type.

#### **Classical Non-Accommodating Cells (cNAC)**

Non-Accommodating Cells, which begin to spike with the onset of stimulus, which do not produce bursts and which do not display a delayed response, were classified as classical Non-Accommodating Cells (cNAC) (**Fig. 1a-b**). These were the most common e-type among L1 cells (n = 41, 40%).

#### **Bursting Non-Accommodating Cells (bNAC)**

Non-Accommodating Cells that display a burst on the onset of stimulus are defined as bursting Non-Accommodating Cells (bNAC; n = 25, **Fig 1a-c**). We identified two subtypes of these cells. The first subtype (n = 15) consists of bNACs that respond to the stimulus with four rapid spikes with a mean ISI of less than 25 ms.

A second subtype of bNAC (n = 10), displayed a 'doublet' of spikes (a pair of action potentials with a maximum ISI of 25 ms) at the beginning of firing.

#### **Classical Stuttering Cells (cSTUT)**

Cells with a poorly fitted regression line (sum of RMS error greater than 30) and at least one "silent period" of more than 100 ms were classified as classical Stuttering Cells.

13% of L1 cells ( $n = 14$ ) belonged to this class. The mean sum of the RMS error for these was 339.05. The average duration of the silent periods was 193.43 ms and the average ISI during spiking was 38.2 ms (**Fig 1a-d**).

### **Classical Irregular spiking cells (cIR)**

Cells with a poorly fitted regression line, which did not meet the criteria for cSTUT, were classified as Classical Irregular Spiking Cells. 7% of L1 cells ( $n=8$ , **Fig 1a-e**) belonged to this class. The mean of the RMS error for these cells was 46.46.

**Figure 1b** shows an example set of traces from a cNAC cell that was used to extract typical single cell electrophysiological features (**Table I**) for further grouping and analysis.

Readers will note that our classification does not reproduce all the e-types identified by other authors, for instance the Late Spiking (LS) cells identified by Chu et al., (Chu and Hablitz, 2003). We observe that several alternative classifications are based on the use of stimulation currents around the threshold value. In our own work, we observed that repeated stimulation with these currents produces highly variable spiking behaviour. Chu et al., (Chu and Hablitz, 2003). We therefore used a square pulse stimulus of 50 pA and varied the amplitude of the pulse until it produced a single AP. The same scaling was used to scale the amplitudes of all subsequent stimuli. This procedure ensured replicability, producing a reliable and parsimonious classification scheme.

### **Electrophysiological Circuitry**

Multi-neuron patch-clamp recording from pairs of neurons detected 82 electrical connections (gap junctions) and 248 chemical synaptic connections, all displaying hyperpolarising GABAergic-like IPSPs. For the study reported below, we selected cells with AP amplitudes greater than 50 mV and Access Resistance less than 10 M $\Omega$ .

#### **Electrical connections**

To detect the presence of gap junctions, we injected a hyperpolarising step current pulse (50 to 100 pA) into one cell in each pair and measured the hyperpolarised response from the other (**Fig. 2a**). The average coupling co-efficient (the ratio of the amplitude of the postsynaptic response to the presynaptic response) was  $0.0543 \pm 0.028$  (mean  $\pm$  SE). All recorded gap junctions (82/2727 pairs; 3% probability) conducted bi-directionally, with no significant differences between conductances in the two directions

(coupling coefficients  $0.052 \pm 0.02$  and  $0.056 \pm 0.03$  respectively) and were therefore classified as symmetrical gap junctions.

### Synaptic connections

For further analysis, we selected 142 out of 248 connections with IPSP amplitudes greater than 1 mV after 5 repetitions of the stimulation protocol.

In 32 connections a single AP was sufficient to evoke IPSPs, always with rise times less than 60 ms ( $28.7 \pm 15$  ms; mean  $\pm$  S.D) (**Fig 2b**). However, the majority of connections ( $n = 110$ ) only responded to trains of stimuli, at a minimum frequency of 40Hz, usually but not always with rise times between 60 and 379 ms ( $159.45 \pm 60.23$  ms; mean  $\pm$  S.D).

An analysis of IPSP latencies showed a distinction between a group of connections with a mean latency of  $4.14 \pm 2.47$  ms (mean  $\pm$  S.D,  $n = 111$ ), and a second group with a mean of  $12.89 \pm 2.963$  ms (mean  $\pm$  S.D,  $n = 31$ ) (**Fig 3e**). Decay times varied between 105 ms to 1.26 s ( $336.2 \pm 138.7$  ms; mean  $\pm$  S.D). The CV (coefficient of variation) had a mean value of  $0.38 \pm 0.25$  (mean  $\pm$  S.D).

We also observed a steady decay of IPSP amplitude over repetitions of stimulation (**Fig 4**). This decay persisted despite using varying inter stimulus intervals of 30, 60 and 90 seconds (**Fig 4c**).

Fast rise times and low latencies are characteristic of GABA<sub>A</sub> transmission dynamics. The calculated chloride reverse potential for our ICS was -69 mV. This value is again compatible with our results. Slow rise times and higher latencies suggest a role for GABA<sub>B</sub> transmission, a hypothesis supported by our calculated potassium reversal potential (-102 mV). However, we also observed that in many cases connections with fast rise times and low latencies had reversal potentials close to the typical values for potassium and that connections with slow rise times and high latencies often had reversal potentials around the typical values for chloride.

To clarify the respective contributions of GABA<sub>A</sub> and GABA<sub>B</sub> receptors we performed 44 experiments with perforated patch clamping, a technique that limits cytoplasmic dilution and eliminates amplitude decay. In the seven connections, for which it was possible to obtain stable recordings (pre drug IPSP amplitude = 4.83 mV) we applied specific inhibitors, and measured the resulting IPSPs (**Fig. 5b**). The presence of a GABA<sub>A</sub> antagonist (20  $\mu$ M Gabazine) led not only to reductions in IPSP amplitudes but also completely abolished fast rise times (IPSP amplitude during Gabazine perfusion = 1.66



mV). The introduction of a GABA<sub>B</sub> antagonist (4  $\mu$ M CGP55845) blocked the remaining IPSP amplitude (IPSP amplitude during CGP55845 perfusion = 0.64 mV). After washout, the amplitude of the IPSP recovered almost completely (IPSP amplitude after washout = 3.27 mV).

These results prove that the GABA<sub>A</sub> and GABA<sub>B</sub> receptors are both involved in mediating the synaptic response. The GABA<sub>A</sub> receptors are responsible for fast rise times and most of the amplitude of the IPSP. The GABA<sub>B</sub> receptors are responsible for slow rise times.

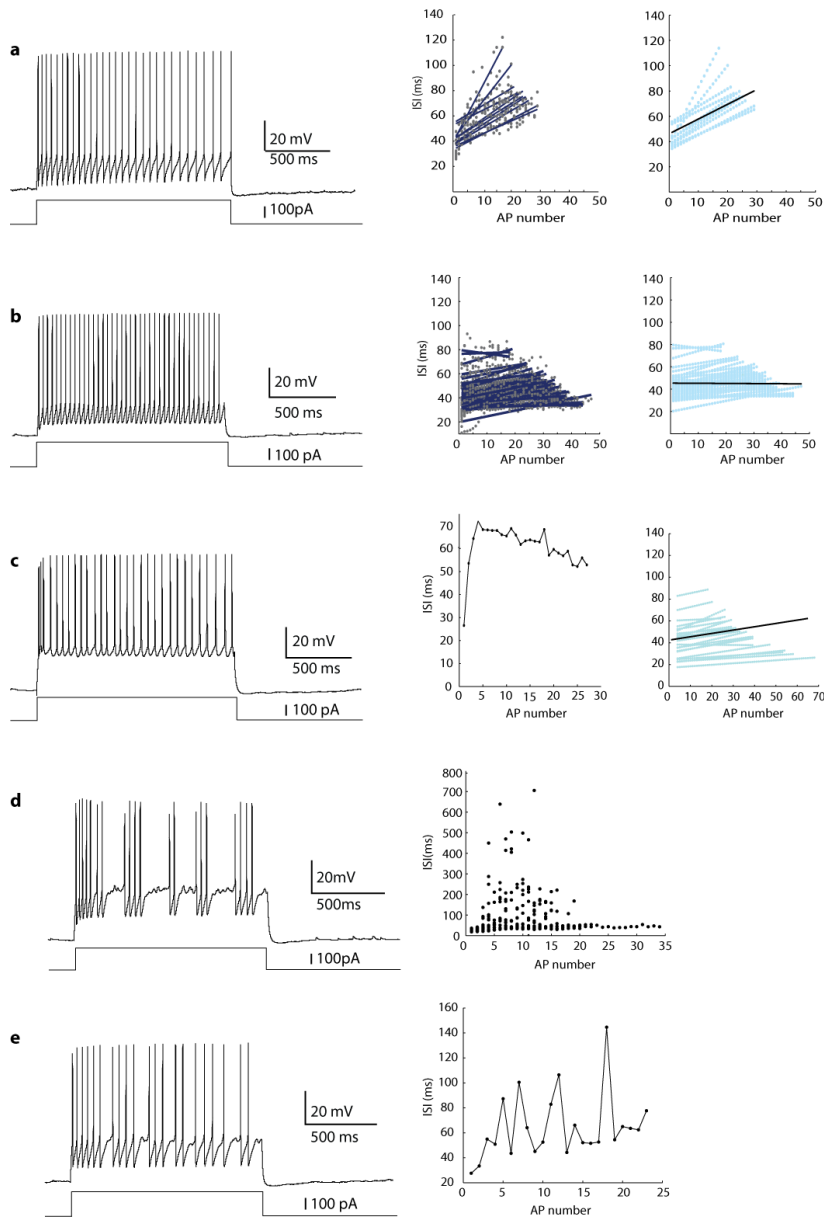


Figure 1

**Figure 1** (a) Characteristic firing pattern for continuous adapting cells (cAC). The first scatter plot on the right plots raw ISI values for successive APs with their linear fits; the second scatter plot shows the grand fit, which has a slope of 1.168. All patterns with slopes clearly greater than 1 were taken as adapting. (b) Firing pattern for continuous non-adapting cells (cNAC) with scatter plots of ISI values, and grand fit. Both fits show minimum changes in ISI values (slope = -0.013). (c) Firing pattern for burst non-adapting cells (bNAC). The scatter graphs show that ISI values are initially low; they then abruptly peak, after which subsequent ISI values follow a typical non-accommodating trend. The grand fit for the post peak ISIs has a slope less than 1 (0.322). (d) Firing pattern for classical stuttering cells (cSTUT) with episodic action potentials followed by protracted periods of silence. The scatter plot show no meaningful trend and silent periods up to 700 ms. (e) Firing patterns for typical irregular firing cells (cIR) showing irregularly spaced action potentials but with much shorter silent periods than cSTUT.

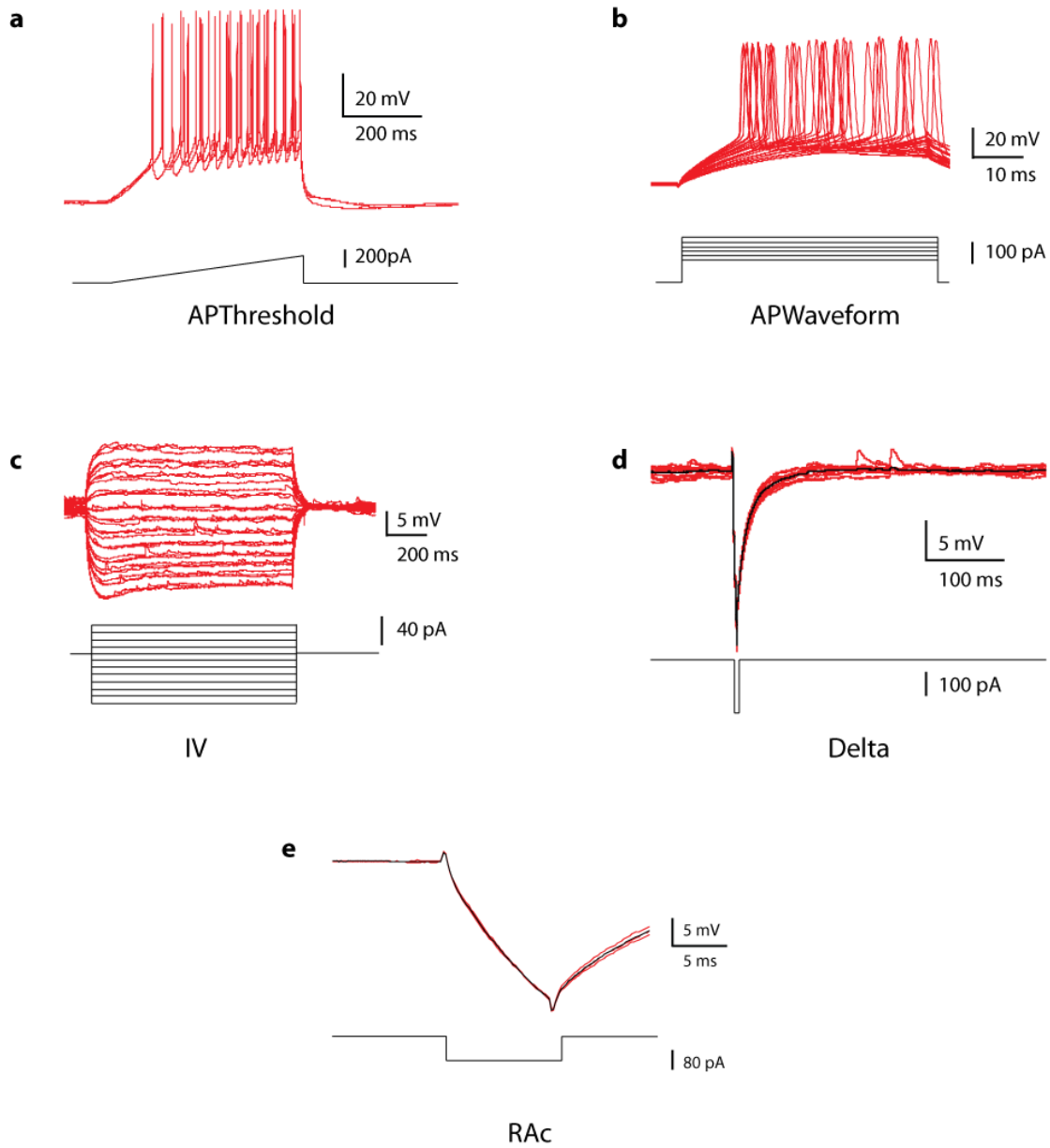


Figure 2

**Figure 2** A sample of current stimuli used as part of the e-code and the voltage responses of a typical cNAC (a) APThreshold is a gradually ramped current stimulus designed to detect the firing threshold of the neuron; (b) APWaveform is a set of square pulses of very short duration, used to study the properties of single APs. (c) a set of subthreshold square pulses used to extract the input resistance of the neuron at peak and steady state voltages (d) The single hyperpolarising Delta pulse provides information about the membrane time constant; (e) RAc is a short hyperpolarising pulse, used to monitor electrical access to the cell, during electrophysiological recordings.

E-parameters	Units	cAC		cNAC		bNAC		cSTUT		cIR	
		mean	S.E	mean	S.E	mean	S.E	mean	S.E	mean	S.E
AP0 amplitude	mV	63.88	5.79	60.85	8.02	60.47	5.34	64.58	5.95	66.94	6.32
AP0 duration	ms	2.53	0.73	2.43	0.34	2.57	0.42	2.66	0.66	2.37	0.58
AP0 half-width	ms	1.29	0.27	1.25	0.18	1.31	0.19	1.32	0.29	1.20	0.26
AP0 rise-time	ms	0.99	0.13	0.98	0.11	0.99	0.10	1.01	0.15	0.97	0.16
AP0 fall-time	ms	1.54	0.61	1.44	0.25	1.57	0.33	1.65	0.53	1.41	0.43
AP0 ahp-time	ms	2.77	2.10	2.99	1.97	2.19	1.82	2.36	1.14	1.98	1.83
AP0 rise-rate	mV/ms	65.75	9.91	63.02	12.42	61.43	7.89	65.93	12.25	70.75	11.43
AP0 fall-rate	mV/ms	45.45	13.17	43.78	10.39	40.02	8.84	42.75	11.63	50.64	12.98
AP0 fast AHP	mV	16.12	3.97	14.46	3.77	12.19	5.51	13.15	4.07	14.69	5.47
AP1 amplitude	mV	63.59	5.26	60.97	7.29	59.41	4.45	61.17	7.59	62.86	3.72
AP1 duration	ms	2.91	0.90	2.76	0.55	3.09	0.70	2.99	0.71	2.74	0.96
AP1 half-width	ms	1.53	0.41	1.45	0.26	1.62	0.34	1.55	0.35	1.46	0.51
AP1 rise-time	ms	1.07	0.17	1.06	0.14	1.09	0.13	1.08	0.18	1.06	0.27
AP1 fall-time	ms	1.84	0.75	1.71	0.45	2.00	0.58	1.90	0.55	1.69	0.69
AP1 ahp-time	ms	1.56	1.57	1.41	1.45	2.71	1.76	2.09	1.26	2.06	1.23
AP1 rise-rate	mV/ms	60.93	11.71	58.91	11.64	55.39	8.75	58.54	14.19	62.68	15.50
AP1 fall-rate	mV/ms	39.45	14.56	37.98	10.27	32.27	9.99	34.90	10.61	42.18	14.80
AP1 fast AHP	mV	20.38	5.45	17.27	7.59	13.46	5.51	16.31	3.52	16.67	4.46
Input resistance for peak	MOhm	396.67	270.57	347.76	102.35	374.98	143.95	293.88	97.10	257.75	115.85
Input resistance for steady-state	MOhm	334.44	218.95	323.47	92.83	346.31	128.15	281.00	87.19	249.72	104.28
Time constant for Delta pulse	ms	17.77	6.70	18.84	6.42	23.67	8.47	16.37	5.45	17.37	12.42
AP threshold	mV	-37.31	4.71	-35.66	8.74	-37.01	6.49	-32.61	15.58	-39.60	3.21
sAHP maximum	mV	9.15	3.19	8.08	3.89	6.18	2.34	2.92	15.62	8.59	3.13
Minimum current to threshold	pA	35.44	29.49	41.82	31.51	37.52	17.13	38.62	14.83	42.77	25.59

Table 1

**Table 1** Values of the electrophysiological parameters for each electrophysiological cell-type in L1. These parameters were extracted automatically from the responses of the cells to a standardised set of electrical stimuli. cAC: n = 11, cNAC: n = 41, bNAC: n = 25, cSTUT: n = 14, cIR: n = 8.

E-code parameters	cNAC vs bNAC	cAC vs bNAC	bNAC vs cIR
AP1 amplitude	0.50	0.45	0.09
AP1 duration	0.14	0.85	0.33
AP1 half-width	0.36	0.95	0.28
AP1 rise-time	0.94	1.00	0.70
AP1 fall-time	0.06	0.82	0.25
AP1 ahp-time	0.02*	0.17	0.87
AP1 rise-rate	0.80	0.56	0.09
AP1fall-rate	0.23	0.20	0.02*
AP1 fast AHP	0.01*	0.01*	0.16
AP2 amplitude	0.85	0.14	0.31
AP2 duration	0.03*	0.47	0.25
AP2 half-width	0.03*	0.52	0.33
AP2 rise-time	0.44	0.77	0.72
AP2 fall-time	0.01*	0.43	0.19
AP2 ahp-time	0.06	0.32	0.85
AP2 rise-rate	0.43	0.24	0.20
AP2 fall-rate	0.02*	0.07	0.03*
AP2 fast AHP	0.15	0.02*	0.45
Input resistance for peak	0.13	0.97	0.05
Input resistance for steady-state	0.13	0.57	0.07
Time constant for Delta pulse	0.00**	0.03	0.10
AP threshold	0.40	0.97	0.34
sAHP maximum	0.17	0.05	0.20
Minimum current to threshold	0.80	0.61	0.77

Table 2

**Table 2** Pairwise comparisons between electrophysiological cell-types in **Table I**.  $P < 0.05 = *$  and  $P < 0.01 = **$  (Student's T). Table shows comparisons with at least significant differences for at least 2 features.

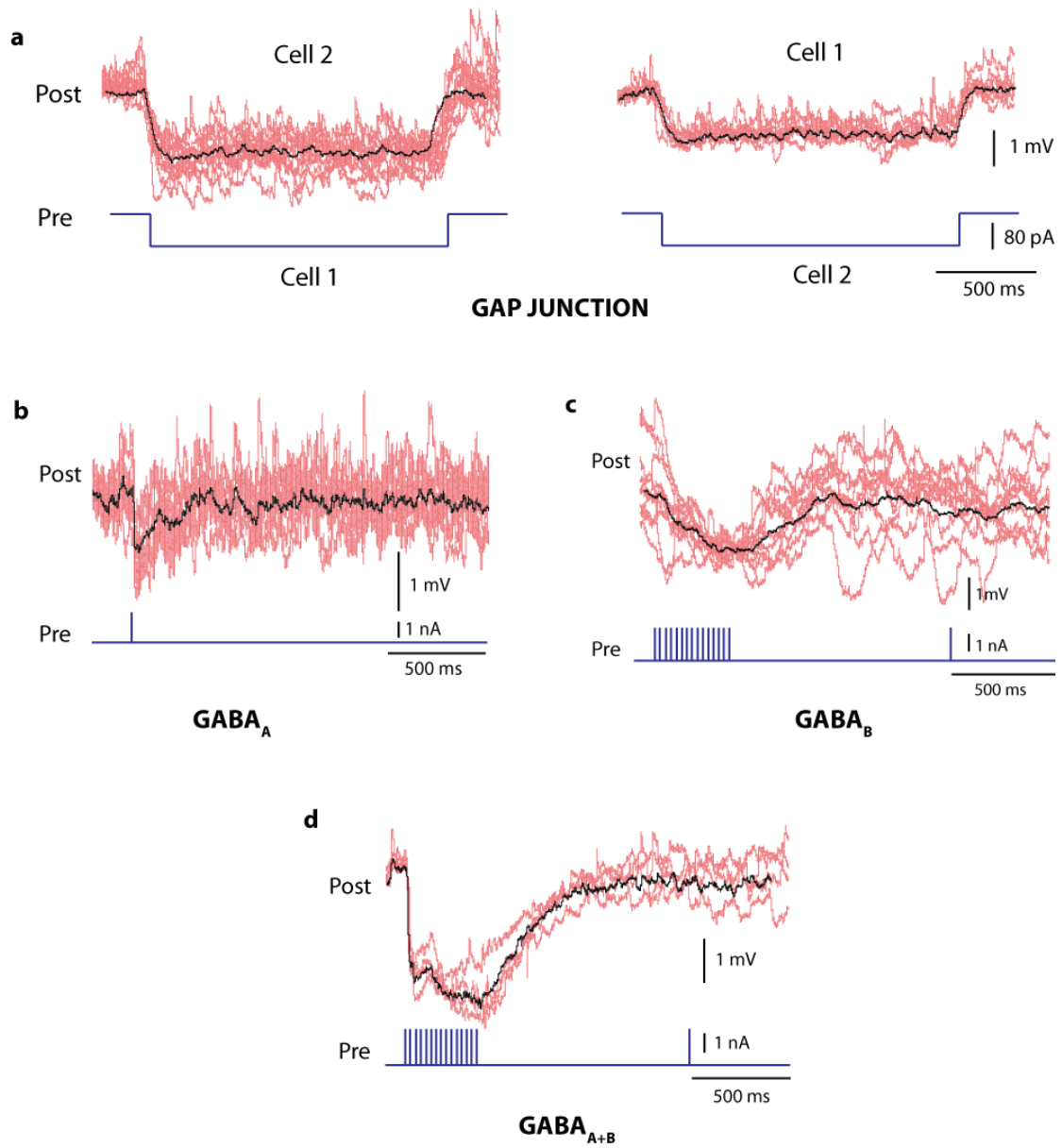


Figure 3

**Figure 2** Examples of electrical recordings from pairs of cells connected by (a) a gap junction; connections mediated by (b) GABA<sub>A</sub>, (c) GABA<sub>B</sub> and (d) GABA<sub>A+B</sub>; individual traces in red; mean values in black. All post synaptic cells were clamped at -57 mV.

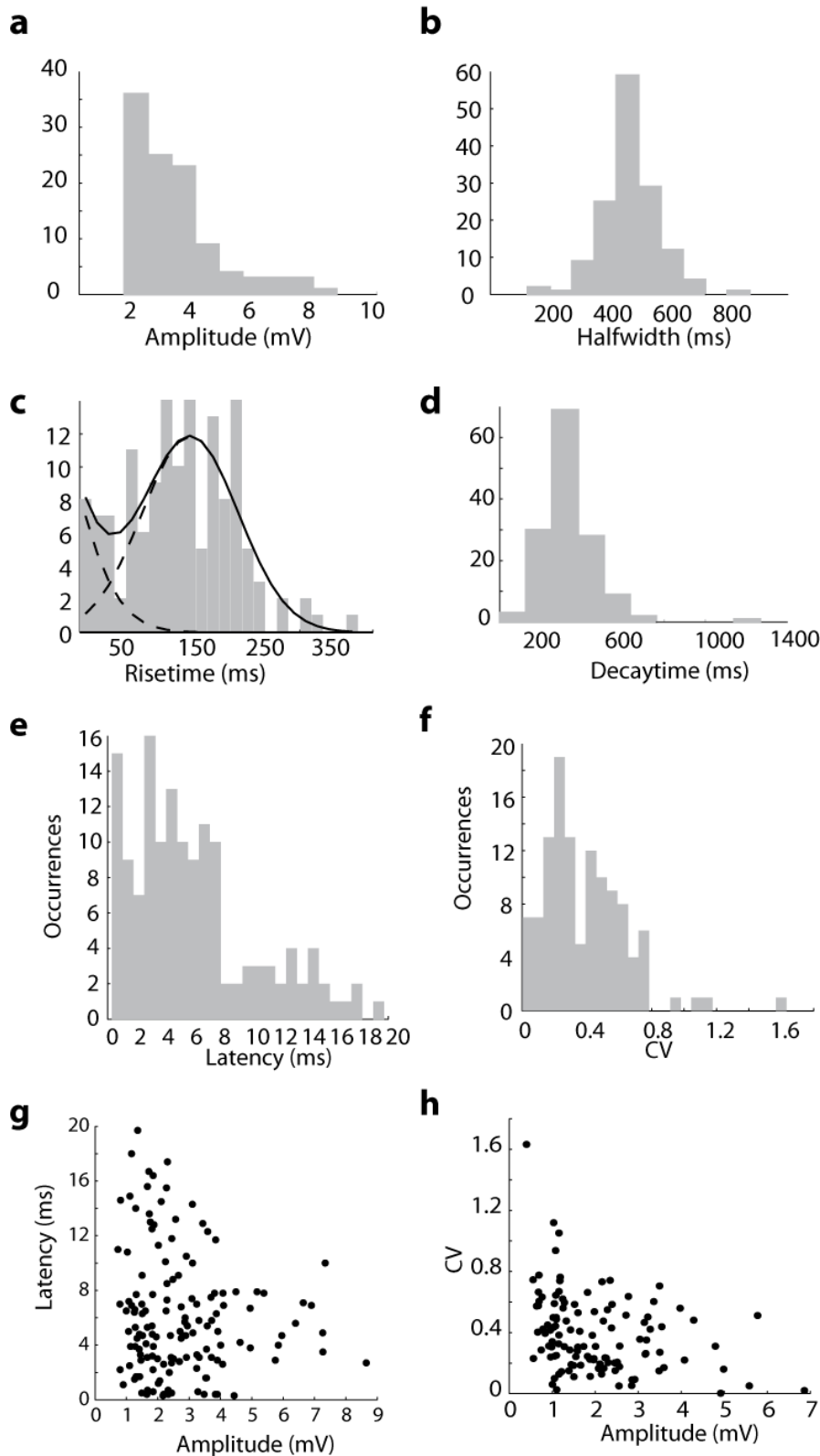


Figure 4

**Figure 4** Parameters for synapses between L1 cells. (a) distribution of IPSP amplitudes (b) Distribution of IPSP halfwidth, (c) distribution of IPSP risetime (d) distribution of IPSP decay time (e) distribution of PSP latency values (f) distribution of coefficients of variation (f) scatter plot latency against IPSP amplitude scatter with a linear fit and a slope of -0.32 (g) distribution of values for Co-efficient of Variation (CV). The best fit for the rise time histogram in (c) is a double Gaussian, indicating the presence of two populations of GABAergic connections

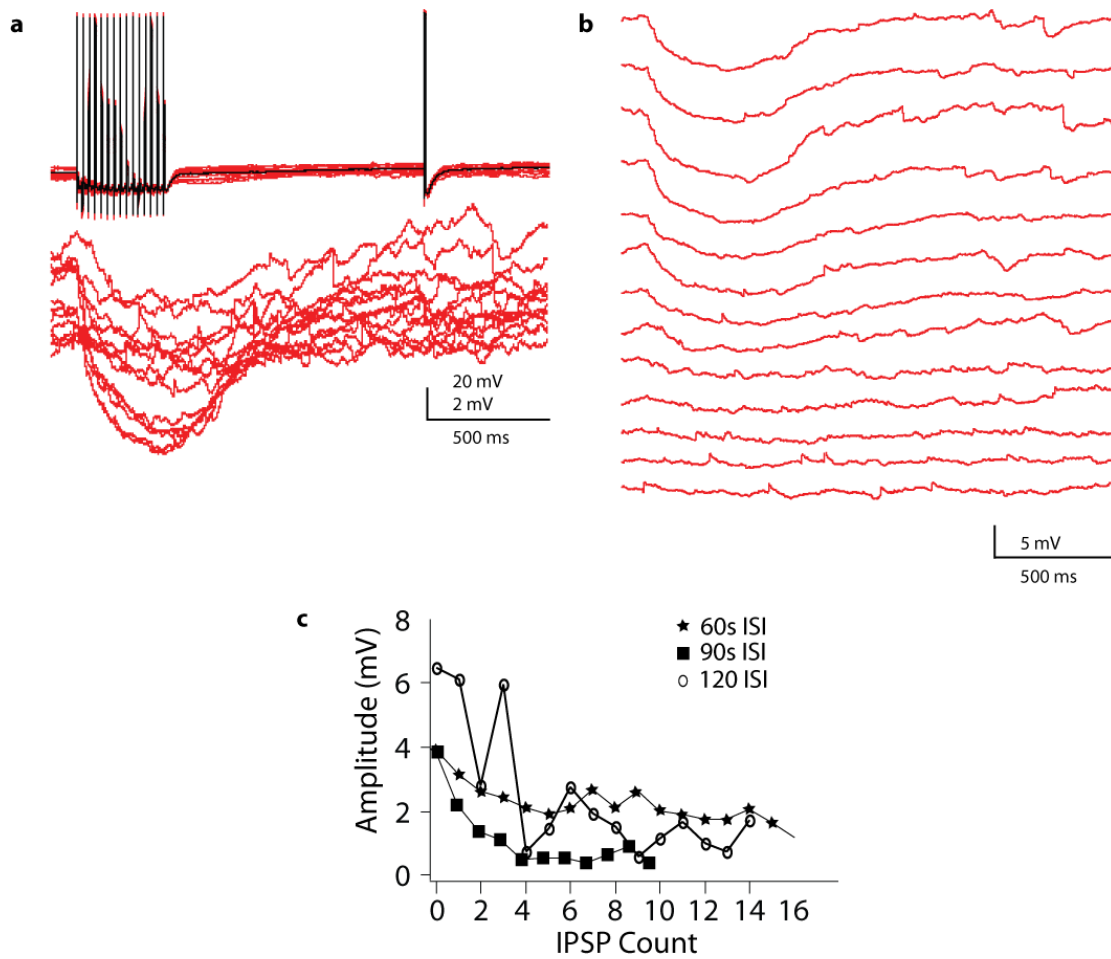


Figure 4

**Figure 4** (a) shows an example of a GABAergic synapse between L1 cells (b) shows the same post synaptic traces as (a) but staggered in offset to show the decay of amplitude over repetitions of the stimulus. (c) shows the decay of IPSP amplitudes over three different values of Inter stimulus Intervals (ISI)



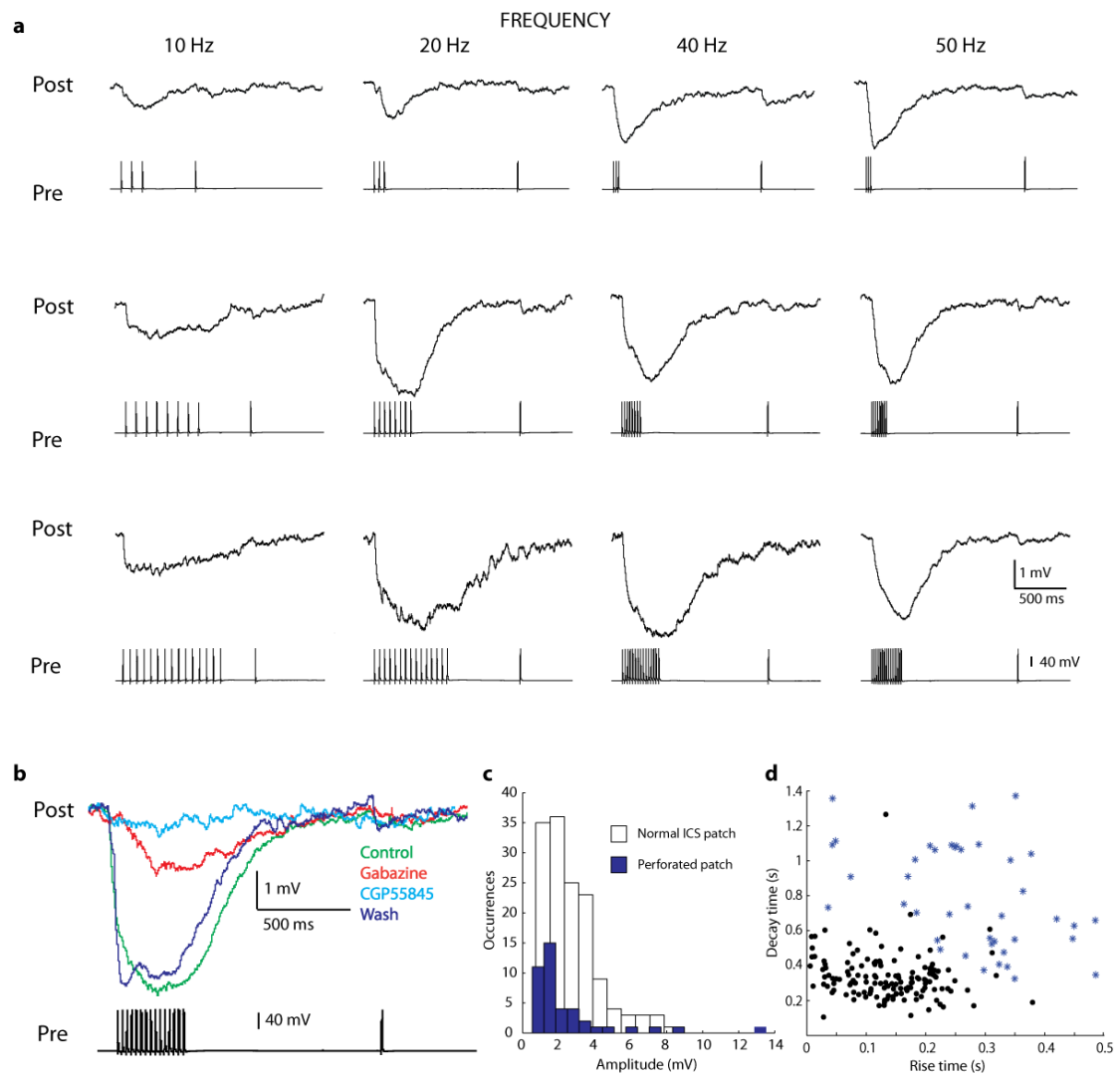


Figure 5

**Figure 5** (a) Frequency analysis of a synaptic connection performed with perforated patch, examples showing variation in spike number (3, 8 and 15) and frequency (10, 20, 40, 50 Hz); All postsynaptic cells were clamped at -57 mV (b) pharmacology performed with Gabazine (GABA<sub>A</sub> blocker) and CGP55845 (GABA<sub>B</sub> blocker); All postsynaptic cells were clamped at -57 mV (c) histogram of the amplitudes of connection measured with normal ICS patch and perforated patch, showing the presence of lower amplitude connections with perforated patch (d) rise and decay times of the connection also differ, possibly due to the perforated patch.

## Chapter 4 Results - Morphology

### Intrinsic morphological properties of single cells

#### Expert-based subjective classification

Out of a total of 158 stained L1 cells, 95 were reconstructed in 3D for morphometric analysis and quantitative comparison. For each neuron, we measured a large set of dendritic and axonal parameters including segment length, segment tortuosity and branch angles (**Table III**). On this basis, we produced an initial subjective classification of cells into the following types: Neurogliaform Cells with dense (NGC-DA) and sparse local axonal arbourisation (NGC-SA), Horizontal Axon Cells (HAC), Descending Axon Cell (DAC); Large Axon Cell (LAC) and Small axon cell (SAC). We also identified one Cajal-Retzius cell.

Cell type	Total number	Percentage (%)
NGC-DA	33	20.88
NGC-SA	26	16.45
HAC	37	23.41
DAC	25	15.82
LAC	19	12.02
SAC	17	10.75

#### Neurogliaform Cells with dense axonal arbours (NGC-DA)

NGC-DA cells, very similar to the Neurogliaform cells reported in other cortical layers, were identified by their small dense arborisation and curvy axonal and small dendritic segments ( $26 \pm 2 \mu\text{m}$ ). (Kawaguchi and Kubota, 1997; Kisvárdy et al., 1990; Szabadics et al., 2007) (**Fig 6a**). With a maximum horizontal extension (H) of  $122 \pm 9 \mu\text{m}$  and a maximum vertical extension (V) of  $133 \pm 12 \mu\text{m}$ , these were the smallest cells we found in L1 (**Table III**).

#### Neurogliaform Cells with Sparse Axonal Arbours (NGC-SA)

NGC-SA neurons showed axonal branching patterns similar to NGC-DA, in terms of segment length, curviness, tortuosity, and branch angles. However, NGC-SA had

sparser distributions of arbourisations, significantly shorter total lengths, lower segment numbers and shorter maximum vertical extensions. The dendritic arbourisations were also wider, showing larger horizontal extensions, longer segment lengths and smaller branching angles (**Table III**).

### **Horizontal Axon Cells (HAC)**

HAC neurons were characterised by large horizontal axonal arbourisations and large segment lengths (axon segment length =  $67 \pm 3 \mu\text{m}$ ). As a result, their Horizontal/Vertical extent (H/V) ratio (H:  $826 \pm 47 \text{ mm}$ , V:  $202 \pm 16 \text{ mm}$ ) was higher than for any other cell type.

### **Descending Axon Cells (DAC)**

With axonal collaterals that descend into deeper layers, commonly reaching layer 4 or 5, these neurons correspond to the descending axon cells reported in previous studies (Hestrin and Armstrong, 1996) (**Fig. 6b, Table III**). Their horizontal and vertical axonal arbourisation patterns were the largest of any cell type. They also showed the largest dendritic segment lengths.

### **Large Axon Cells (LAC)**

The axons of LACs displayed the longest length, the highest segment number and the highest maximum branch order we observed in any cell type (**Fig. 6b, Table III**). LACs', axonal collaterals often spread into layers 2 and 3 (6/10 cells). LAC dendrites displayed the highest segment number (i.e. higher frequency of branching) observed in any cell type.

### **Small Axon Cells (SAC)**

SACs had the lowest axonal segment number, the smallest H/V ratio, the lowest axonal tortuosity values, the lowest maximum axonal branch order (MABO), the largest axonal branch angles, the lowest bouton density and the lowest total axonal lengths of any cell type (**Fig. 6b, Table III**). Some SACs (4/11 cells) projected one to two axonal collaterals into layers 2 and 3.

### **Rare cell types**

Out of 160 stained cells, we found one Cajal-Retzius cell like Cell (CR-like C). This is consistent with the fact that the CR cell type appears in the L1 of very young

animals and disappears around P10 (Hestrin and Armstrong, 1996).

### **Objective analyses**

To refine and qualify our initial classification of morphological cell types we performed a series of objective analyses as described below.

### **Variance analysis**

A systematic analysis of individual feature variance values made it possible to identify outliers and incomplete cells. Out of a total of 91 cells, two displayed feature values far outside the distributions for the other cells. In particular, the densities of their basal dendrite were respectively 8.93 and 2.57 standard deviations from the mean (**Fig 7**). These cells were considered as outliers and excluded from our subsequent analyses.

### **Feature power analysis**

Preliminary tests suggested that our original subjective feature set might not be sufficient to allow fully automated separation among different morphological cell types. We, therefore enriched our additional feature list with a large set of new features commonly used in the literature (**Table IV**) and used feature power analysis to rank them according to their ability to cluster the dataset. This analysis compares the between-group variance with the within-group variance of each feature to determine the ones that are most discriminative. Features that are most powerful in their discrimination appear on the upper left corner of the plot. **Fig. 8a** shows the results of one such analysis. In the analyses reported below we used the full feature set, excluding two low power features (43 and 22), which we removed to ensure clarity and robustness (**See Fig 9b and Table IV**)

### **Principal Component Analysis (PCA)**

The central idea of principal component analysis (PCA) is to reduce the dimensionality of a dataset consisting of a large number of inter-related variables, while retaining as much as possible of the variation present in the dataset. The initial uncorrelated principal components (PCs) are transformed and ordered as per the amount of variation retained (Jolliffe, 2002). To generate an initial unsupervised analysis, we normalised the raw feature dataset and performed a PCA. More than 25 % of the total variance in the dataset was explained by the first principal component. Moreover, we did not see a clear separation of any groups of cells (**Fig. 8b**).

## **Linear Discriminant Analyses (LDA)**

For our final objective classification, we applied LDA, a supervised method that reduces the dimensionality of a given dataset, while preserving as much discriminatory information as possible i.e. maximising the ratio of between-class to within-class variance. The result is a weight vector which, when applied to features, produces the maximum possible separation between groups (Krzanowski, 2000).

In LDA, it is necessary to define the number of clusters to be generated. Using the same number of six categories as in the subjective classification, HAC, DAC and LAC cells separated very clearly. However SAC and the NGC cells were not well separated (**Fig.8d**). Since the DAC group was the best separated cell type, we removed DAC cells from the dataset and re-ran the LDA with five groups. This resulted in a better separation of NGC-DA and LAC but NGC-SA and SAC still clustered together. The results of the classification are given in **Fig. 8c**.

**Figure 9c** shows LDA of the remaining dataset, after the removal of both DAC and HAC. This results in a clear separation of the remaining groups – SAC, LAC, NGC-DA and NGC-SA.

## **Morphological Circuitry**

### **Gap junctions**

To verify the morphological cell types involved in gap junctions, we selected four electrically coupled stained cell pairs. Of the four pairs, one involved two LACs; two pairs involved a LAC and a HAC and a LAC and a DAC, respectively; one involved a DAC and an NGC-DA. We reconstructed one electrically and synaptically coupled L1 pair (**Fig 10a**). Among the eleven putative coupling contacts, four were on the dendrites (**Fig 11** for zoomed in views). Seven contacts involved the axonal collaterals of the two neurons.

### **Synaptic connections**

Among eighteen pairs of connected L1 neurons from fourteen well-stained arbourisations, four neuron types (HAC, DAC, NGC-DA and LAC) were found to form GABAergic synaptic connections. In most cases, synapses were between neurons of the same type (11/18 pairs, 61%), mainly HACs and/or DACs (8/11 pairs, 73%), or NGC-DAs (3/11 pairs, 14%). All connections between different types of neurons (7/18 pairs,

39%) involved HAC and/or DAC cells, mostly as postsynaptic cells (5/7 pairs). LAC (3/7 pairs) and NGC-DA (2/7 pairs) were often presynaptic cells.

Five pairs of L1 connected neurons were reconstructed. These cells had an average of 9.2 putative synapses per pair on the soma and dendrites of the postsynaptic cell. A high fraction (39%) of putative synapses was formed on the soma. This kind of contact was observed in four out of five reconstructed pairs. (**Fig 12** for zoomed in views). **Fig 13** shows the electrophysiological recordings from these pairs of connected cells

### **Morphoelectrical types**

Combining morphological and electrophysiological classification provides a more comprehensive view of the diversity of L1 cells than either of these schemes taken on its own. Out of 38 cells for which we obtained high quality staining and electrophysiological data, 28 (73.6%) expressed a cNAC firing pattern. The most common morphological types were HAC and NGC-DA, each represented by 10/38 cells (26.3%). Combining these two parameters, the most common morpho-electrical types (ME-type) were NGC-DA - cNAC and HAC-cNAC (7/38; 18.4% each). The next most common ME-types were LAC- cNAC and and NGC-SA - cNAC.

Some firing patterns appeared only in specific morphological types. Thus cAC firing patterns were found only in NGC-DAs, SACs and LACs; the cSTUT type was found only in NGC-DAs, and the cIR type only in HACs (**Figs 14a, 14b and 15**).

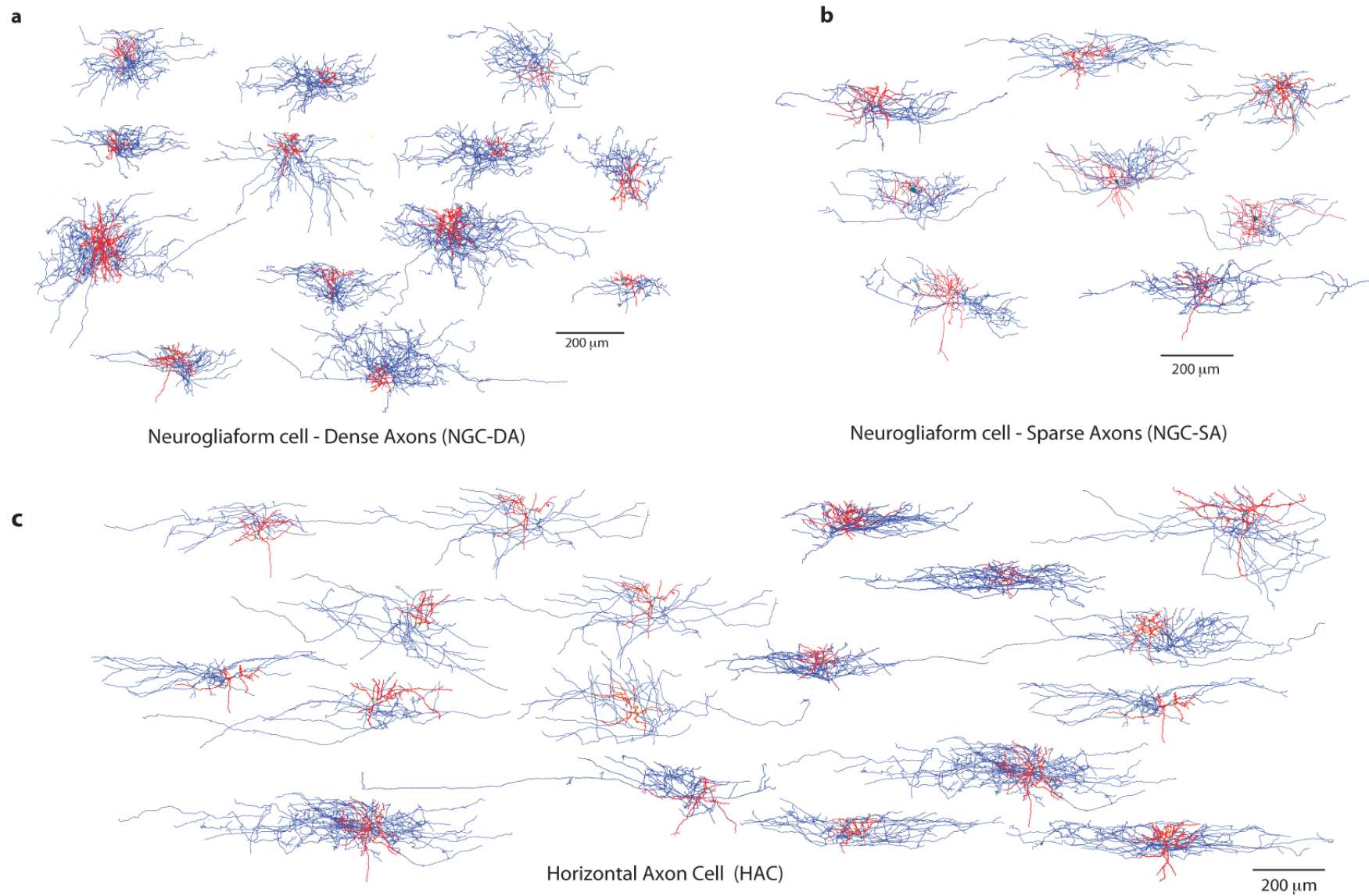


Figure 6a

**Figure 6a** Three of the six major morphological cell types (subjective classification). (a) typical neurogliaform cells with dense axonal arbourisation (NGC-DA). (b) atypical neurogliaform cells with sparse axonal arbourisation (NGC-SA). (c) Horizontal Axon cells (HAC). Dendrites are shown in red and the axonal arbour in blue.

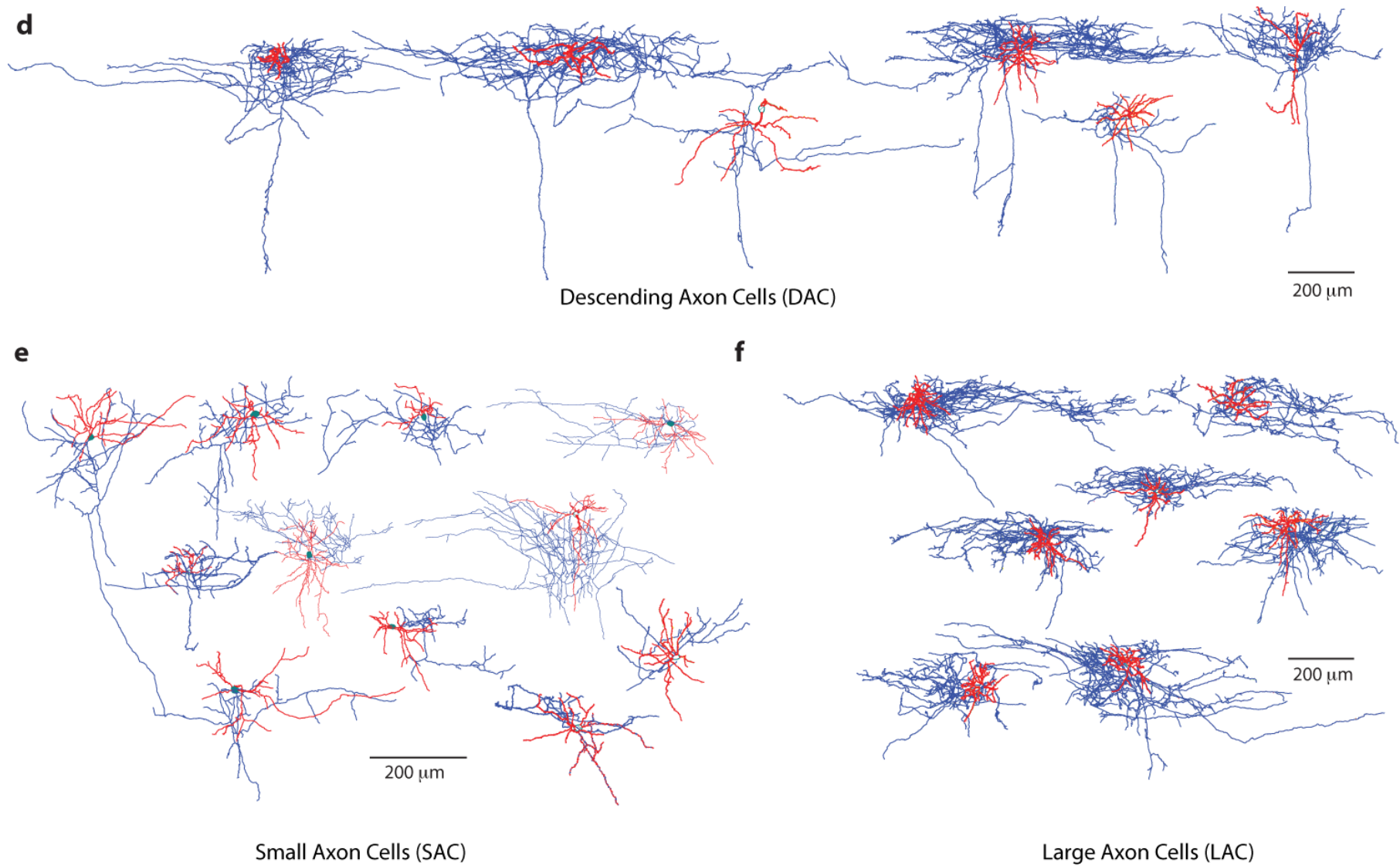


Figure 6b

**Figure 6b** Three of the six major morphological cell types as classified by subjective classification. (d) HACs with a descending axon (DAC) (e) Dense and (f) small axon cells (LAC and SAC) Dendrites are shown in red and axonal arbour in blue



	Name	Variance	Var Ratio
1	Soma CSA	0.81	0.11
2	Basal number trunks	0.76	0.05
3	Basal mean trunk diameter	0.79	0.16
4	Basal number segments	0.72	0.07
5	Basal max branch order	0.73	0.02
6	Basal max path length	0.76	0.26
7	Basal max radial distance	0.76	0.30
8	Basal max degree	0.71	0.06
9	Basal total length	0.79	0.15
10	Basal total surface area	0.79	0.26
11	Basal total volume	0.74	0.28
12	Basal bif mean branch length	0.72	0.34
13	Basal horizontal range	0.75	0.29
14	Basal vertical range	0.81	0.21
15	Dendrite Moment 1 (x)	0.73	0.03
16	Dendrite Moment 1 (y)	0.75	0.03
17	Dendrite Moment 1 (z)	0.76	0.09
18	Dendrite Moment 2 (x)	0.72	0.27
19	Dendrite Moment 2 (y)	0.75	0.24
20	Dendrite Moment 2 (z)	0.77	0.26
21	Dendrite Density	0.31	0.11
22	bdend tortuosity	0.82	0.20
23	hv_ratio_dend (raw h, w)	0.81	0.15
24	Axon mean trunk diameter	0.79	0.07
25	Axon number segments	0.80	0.38
26	Axon max branch order	0.73	0.24
27	Axon max path length	0.78	0.50
28	Axon max radial distance	0.80	0.48
29	Axon max degree	0.80	0.38
30	Axon total length	0.78	0.42
31	Axon total surface area	0.73	0.32
32	Axon total volume	0.64	0.16
33	Axon bif mean branch length	0.78	0.45
34	Axon horizontal range	0.82	0.59
35	Axon vertical range	0.76	0.73
36	Axon Moment 1 (x)	0.76	0.06
37	Axon Moment 1 (y)	0.75	0.11
38	Axon Moment 1 (z)	0.83	0.13
39	Axon Moment 2 (x)	0.83	0.61
40	Axon Moment 2 (y)	0.72	0.62
41	Axon Moment 2 (z)	0.80	0.33
42	Axon Density	0.78	0.48
43	Axon tortuosity	0.79	0.18
44	H/V_ratio_axon (raw h, w)	0.77	0.52

Table 4

**Table 4** Listing of the morphometric features used for the objective analyses (bif = bifurcating)

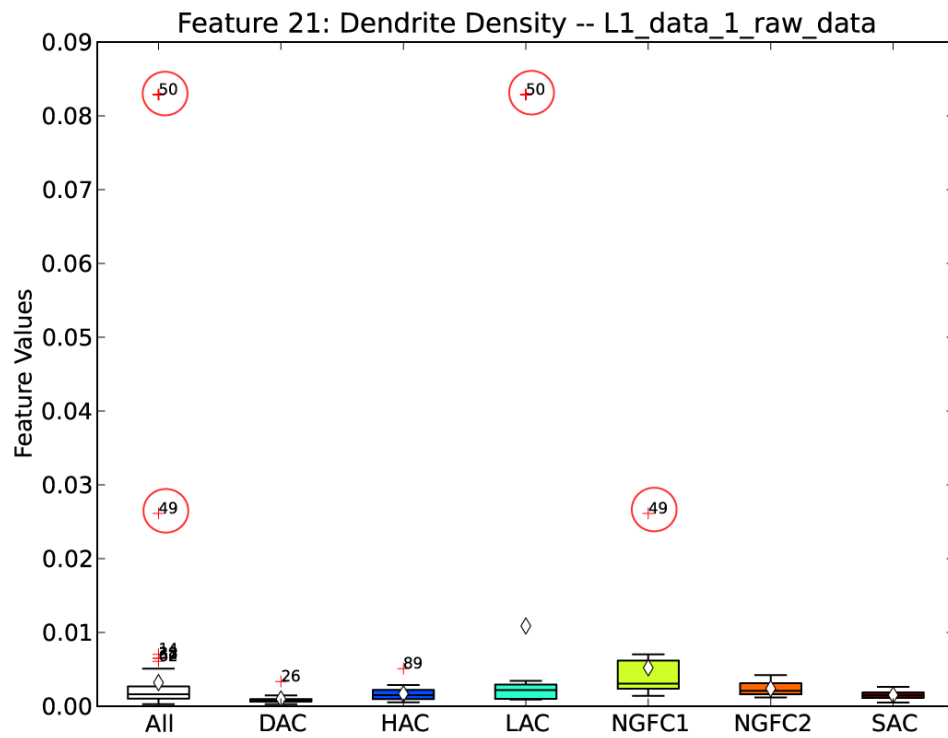


Figure 7

**Figure 7** Boxplot of normalised values for dendrite density, This plot indicates the extreme outlier values found in cells 49 and 50 indicated by red circles.

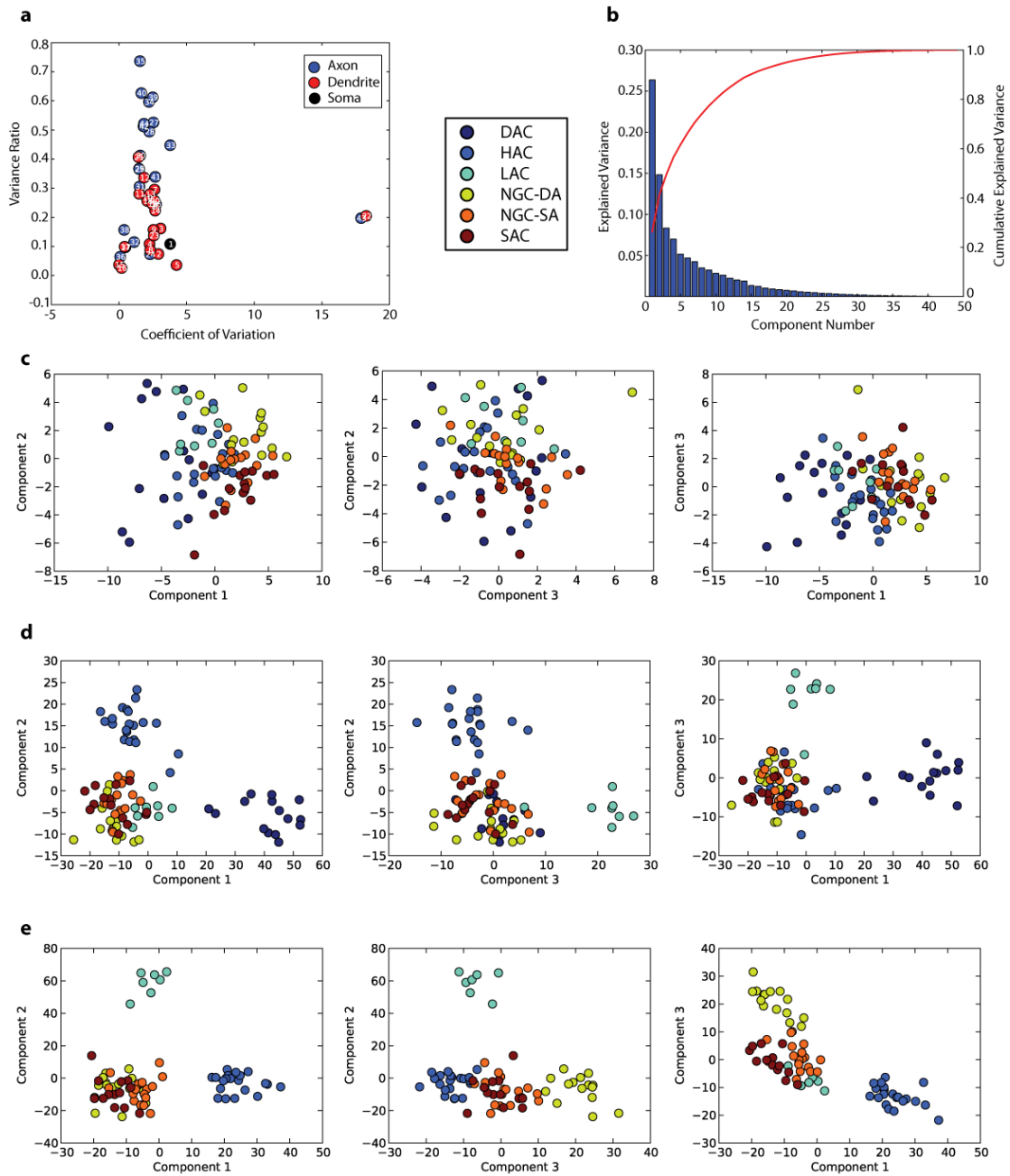


Figure 8

**Figure 8** (a) Feature power analysis: the features with the greatest discriminatory power are all axonal features. (b) Variance explained by PCA components. (c) PCA plots for the standardised dataset (d) LDA plots ( $n=6$ ) showing a significant grouping of DAC, HAC and LAC. (e) LDA plots with  $n=5$  (after removal of DAC) showing better separation of NGC-DA.

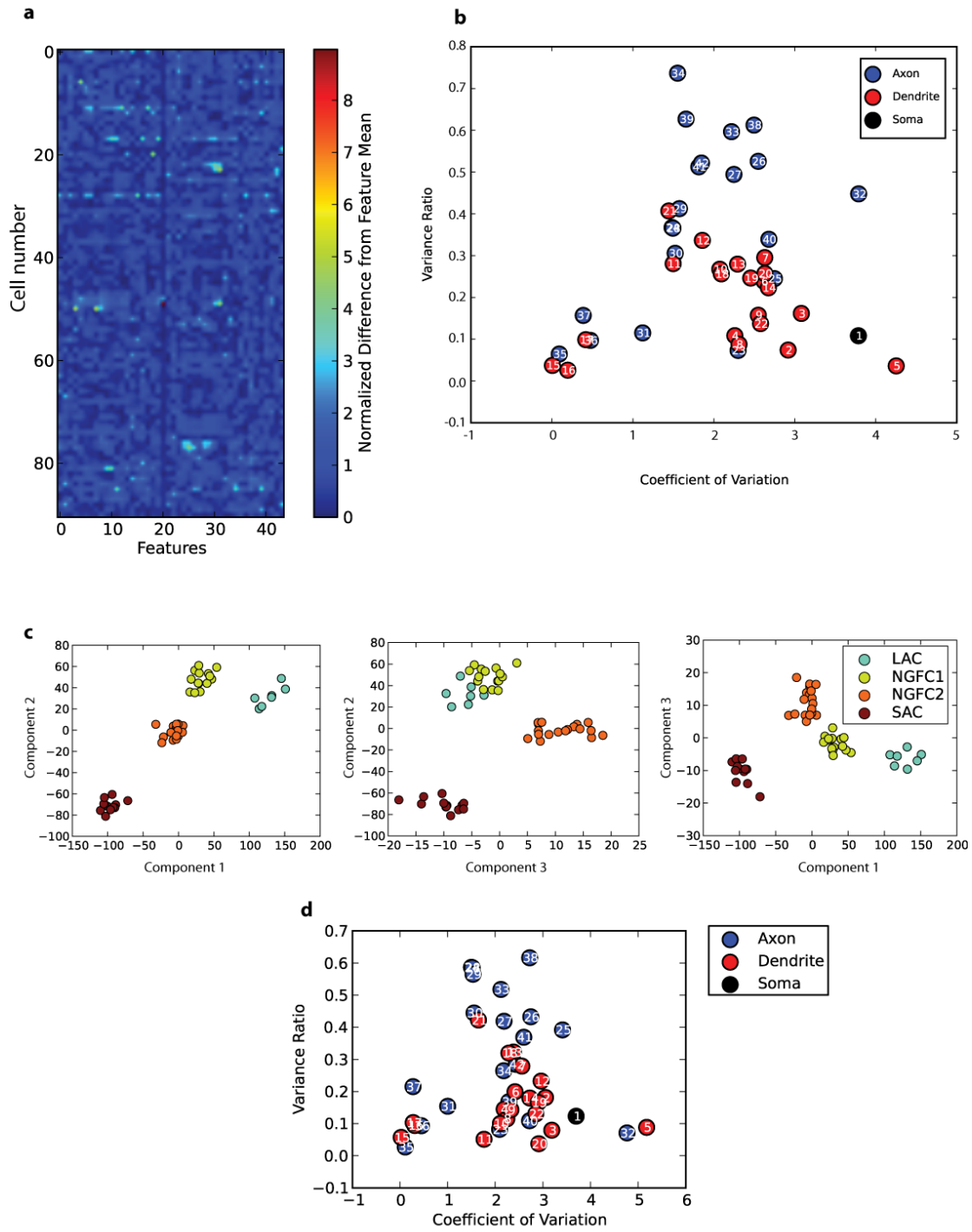


Figure 9

**Figure 9** (a) Variance analysis heatmap showing possible outliers. (b) feature power analysis after the removal of two outlier features (22 and 43) describing dendritic and axonal tortuosity. (c) LDA after removal of DAC and HAC. NGC-DA, NGC-SA, LAC and SAC separate clearly (d) feature power analysis for the LDA in (c).

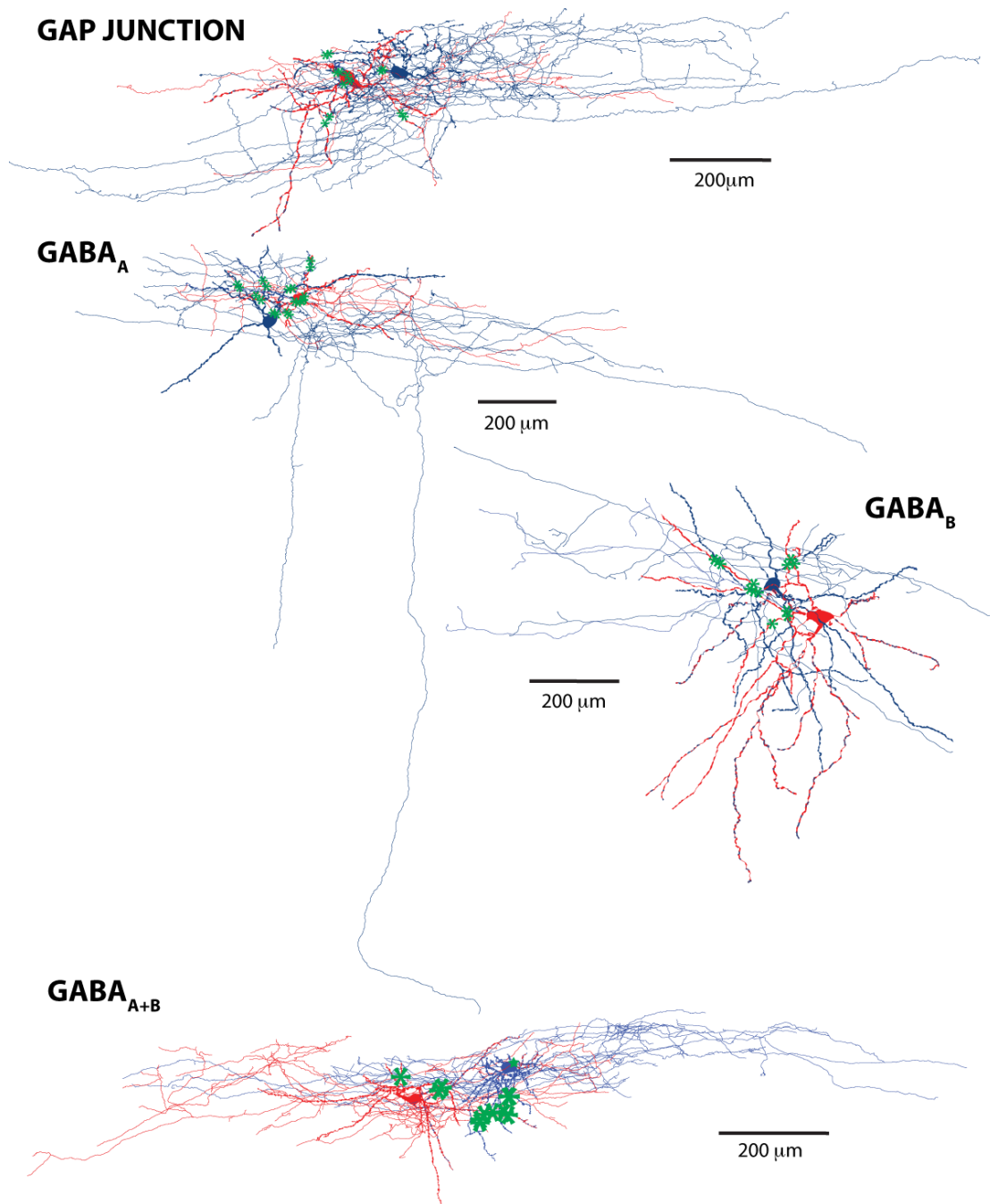


Figure 10

**Figure 10** 3D morphologies for four pairs of connected L1 cells showing the soma positions along with the dendritic and axonal arbours and putative contact points for each kind of connection. Pre-synaptic cells are in red; post-synaptic cells are in blue. Putative contact points are marked with a green asterisk

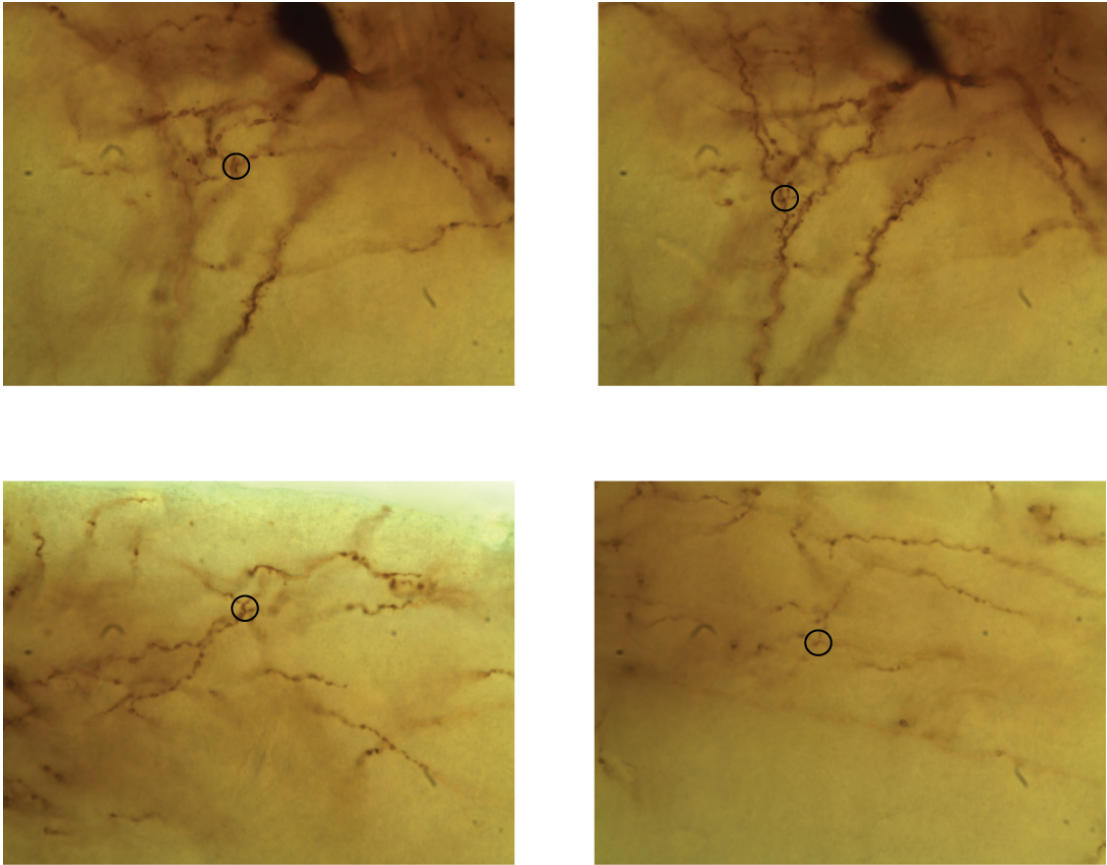


Figure 11

**Figure 11** Light microscope images of putative contact points between a pair of cells connected by gap junction (same pair as **Fig 10**). Black circles indicate the possible contact points identified by visual inspection.

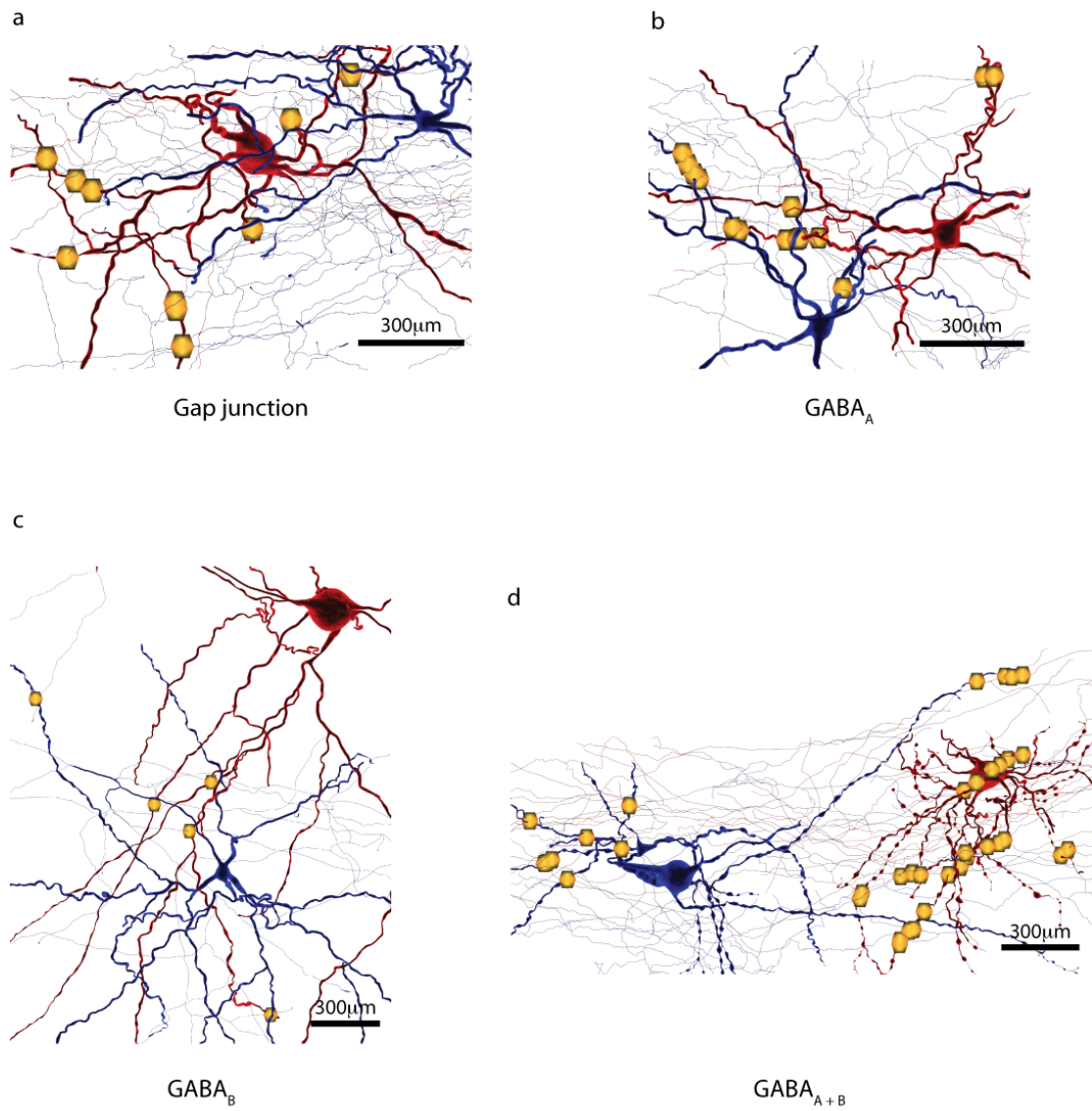


Figure 12

**Figure 12** (a) Close-up of a 3D rendering of the two cells with gap junctions; contact points marked with yellow hexagons. (b) cells with  $GABA_A$  mediated connections (c) cells connected by  $GABA_B$  mediated connections, and (d) cells with connections mediated by both by  $GABA_A$  and  $GABA_B$  receptors.

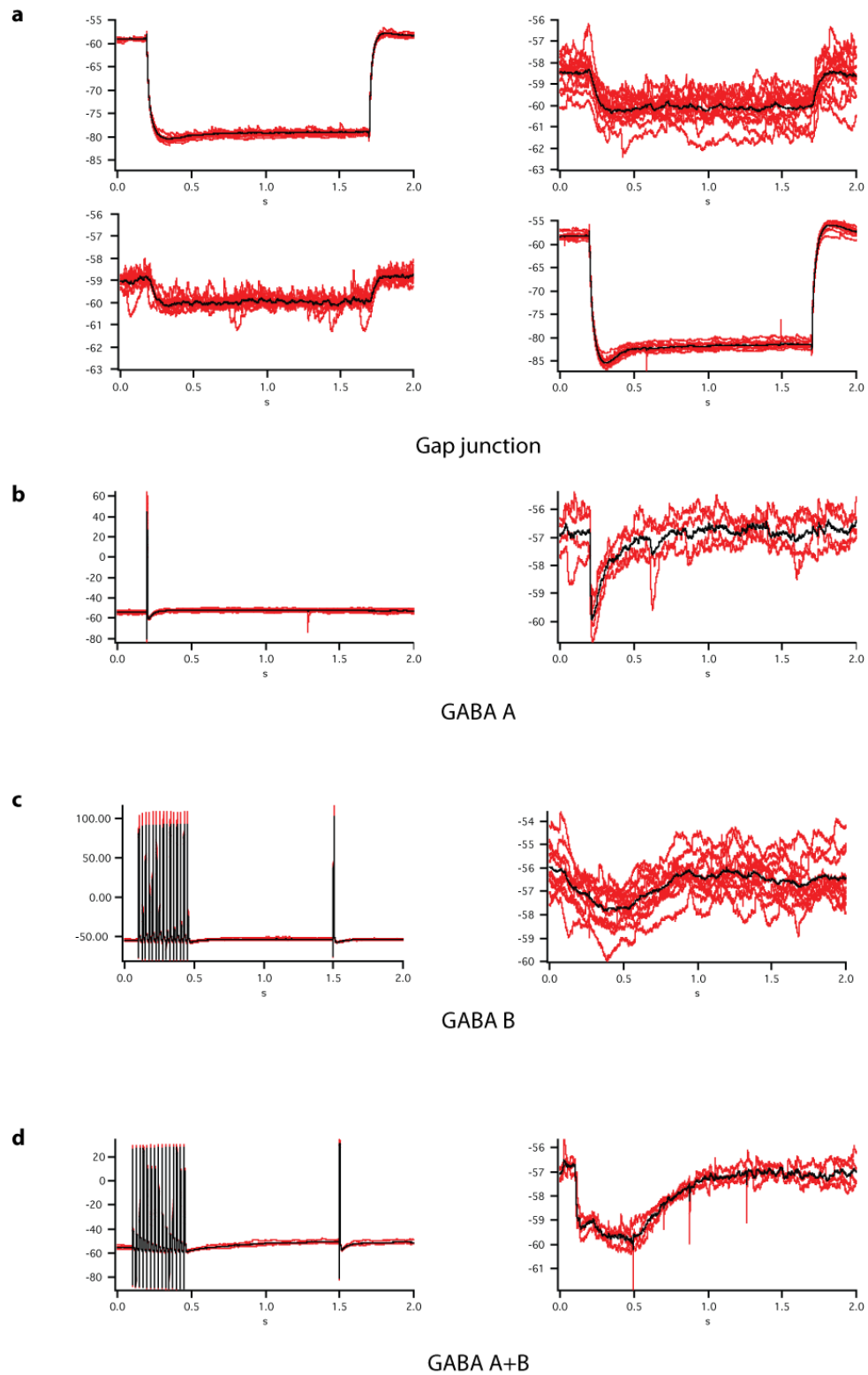


Figure 13

**Figure 13:** (a) Gap junction electrophysiology of the reconstructed pair in **Figure 10** (b) typical GABA<sub>A</sub> post synaptic response elicited by a single pulse for the pair reconstructed in **Figure 10** (c) corresponding GABA<sub>B</sub> IPSP as observed for the reconstructed pair of cells in **Figure 10** (d) GABA<sub>A+B</sub> response as seen between the pair of cells reconstructed in **Figure 10**



# Morphometric properties of layer 1 cells

		NGC-DA	NGC-SA	P	HAC	DAC	P	DLAC	SLAC	P
		n = 17 (15%)	n = 16 (14%)		n = 19 (17%)	n = 16 (14%)		n = 11 (10%)	n = 14 (13%)	
<b>Soma</b>										
	Perimeter(μm)	48 ± 1	49 ± 2	0.56	49 ± 1	51 ± 2	0.34	47 ± 1	43 ± 2	0.10
	Area(μm²)	172 ± 11	178 ± 13	0.68	174 ± 6	191 ± 14	0.27	162 ± 9	135 ± 12	0.07
<b>Dendrite</b>										
	Max horizontal extend (μm)	122 ± 9	191 ± 17	0.00**	227 ± 14	305 ± 48	0.12	211 ± 18	218 ± 26	0.82
	Max vertical extend (μm)	133 ± 12	150 ± 14	0.36	170 ± 14	209 ± 16	0.06	187 ± 17	194 ± 14	0.77
	H/V	1.0 ± 0.1	1.4 ± 0.1	0.01**	1.4 ± 0.1	1.5 ± 0.2	0.80	1.2 ± 0.1	1.2 ± 0.1	0.91
	Dendrite number	5 ± 0.4	6 ± 0.5	0.38	5 ± 0.4	6 ± 0.5	0.38	6 ± 0.5	5 ± 0.4	0.03*
	Length(μm)	1470±239	1821±147	0.19	1808±139	2492±336	0.07	1985±160	1636±149	0.04*
	Tree length (μm)	280 ± 32	336 ± 27	0.16	363 ± 31	479 ± 76	0.16	337 ± 40	322 ± 29	0.76
	Segment length (μm)	26 ± 2	33 ± 2	0.01**	45 ± 3	50 ± 4	0.27	34 ± 1	38 ± 3	0.18
	Segment number	58 ± 9	56 ± 4	0.83	43 ± 4	53 ± 7	0.20	60 ± 6	43 ± 5	0.02*
	Tortuosity	1.28 ± 0.02	1.24 ± 0.01	0.08	1.29 ± 0.02	1.25 ± 0.01	0.08	1.26 ± 0.01	1.18 ± 0.01	0.00**
	Average order	4 ± 0.2	4 ± 0.2	0.40	4 ± 0.2	4 ± 0.3	0.86	4 ± 0.3	4 ± 0.2	0.66
	Maximum Order	7 ± 0.3	7 ± 0.3	1.00	6 ± 0.5	7 ± 0.7	0.76	7 ± 0.5	6 ± 0.3	0.18
	Maximum Angle (deg)	68 ± 2	66 ± 2	0.34	64 ± 1	65 ± 2	0.67	63 ± 2	62 ± 3	0.83
	Planar Angle (deg)	51 ± 1	48 ± 1	0.08	46 ± 2	48 ± 1	0.39	47 ± 1	46 ± 2	0.55
	Local Angle (deg)	59 ± 1	56 ± 1	0.05	60 ± 1	59 ± 1	0.50	56 ± 1	57 ± 2	0.63
	Local Spline Angle (deg)	53 ± 1	50 ± 1	0.02	53 ± 1	53 ± 1	0.69	51 ± 1	49 ± 2	0.32
<b>Axon</b>										
	Max horizontal extent (H) (μm)	481 ± 35	513 ± 33	0.50	826 ± 47	1035 ± 63	0.01**	879 ± 108	411 ± 37	0.00**
	Max vertical extent(V) (μm)	263 ± 33	163 ± 10	0.01**	202 ± 16	602 ± 49	0.00**	316 ± 29	251 ± 40	0.18
	H/V	2.0 ± 0.2	3.3 ± 0.3	0.00**	4.5 ± 0.4	2.0 ± 0.3	0.00**	3.0 ± 0.4	2.0 ± 0.2	0.04*
	Tree length (μm)	11067±1475	6134±655	0.00**	9688±1099	14584±2084	0.04*	15082±1084	3325±543	0.00**
	Segment length (μm)	42 ± 2	45 ± 2	0.38	67 ± 3	60 ± 3	0.15	44 ± 2	45 ± 2	0.79
	Segment number	270 ± 38	142 ± 16	0.00**	155 ± 21	273 ± 46	0.03*	342 ± 26	89 ± 17	0.00*
	Tortuosity	1.30 ± 0.01	1.29 ± 0.01	0.49	1.27 ± 0.01	1.24 ± 0.01	0.08	1.31 ± 0.03	1.22 ± 0.02	0.01**
	Maximum Order	16 ± 1	15 ± 1	0.24	14 ± 1	20 ± 2	0.01**	21 ± 2	12 ± 1	0.00**
	Maximum Angle (deg)	73 ± 1	74 ± 2	0.65	74 ± 2	75 ± 1	0.72	72 ± 2	78 ± 1	0.02*
	Planar Angle (deg)	53 ± 1	53 ± 1	0.53	52 ± 1	52 ± 1	0.79	50 ± 1	55 ± 1	0.01**
	Local Angle (deg)	58 ± 1	60 ± 1	0.31	61 ± 1	62 ± 1	0.64	59 ± 1	61 ± 1	0.47
	Local Spline Angle (deg)	52 ± 1	54 ± 1	0.23	55 ± 1	55 ± 1	0.69	54 ± 1	55 ± 1	0.55
	Bouton Density (number/μm)	0.20 ± 0.01	0.19 ± 0.01	0.52	0.20 ± 0.01	0.18 ± 0.01	0.17	0.20 ± 0.01	0.16 ± 0.01	0.03*

\* P <= 0.05

\*\* P <= 0.01

Table 3

**Table 3** A summary of the morphometric parameters for the six morphological cell-types used for the subjective classification.

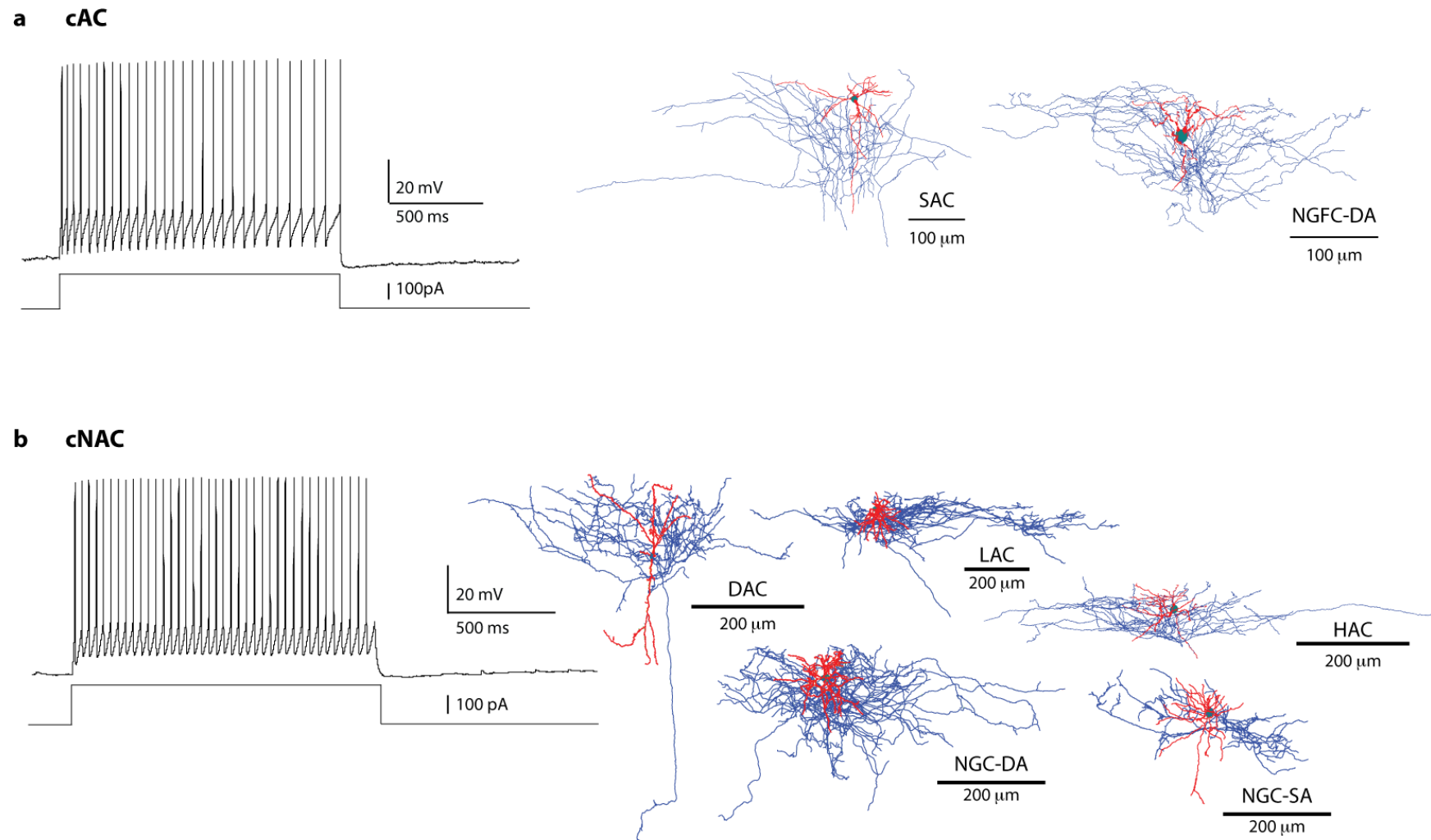


Figure 14

**Figure 14** Firing types seen in L1 with their corresponding cellular morphologies

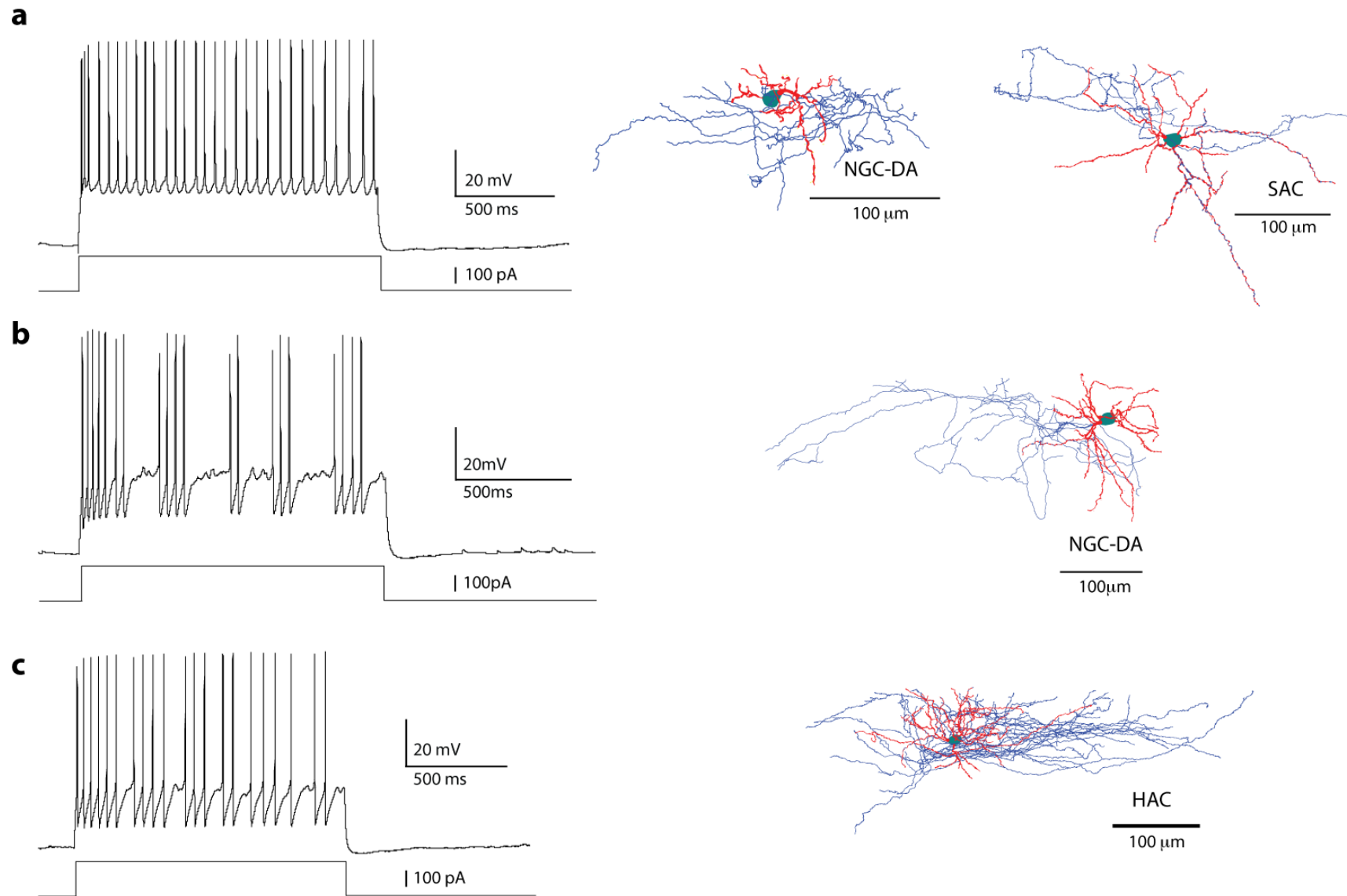


Figure 15

**Figure 15** Firing types seen in L1 with their corresponding cellular morphologies.

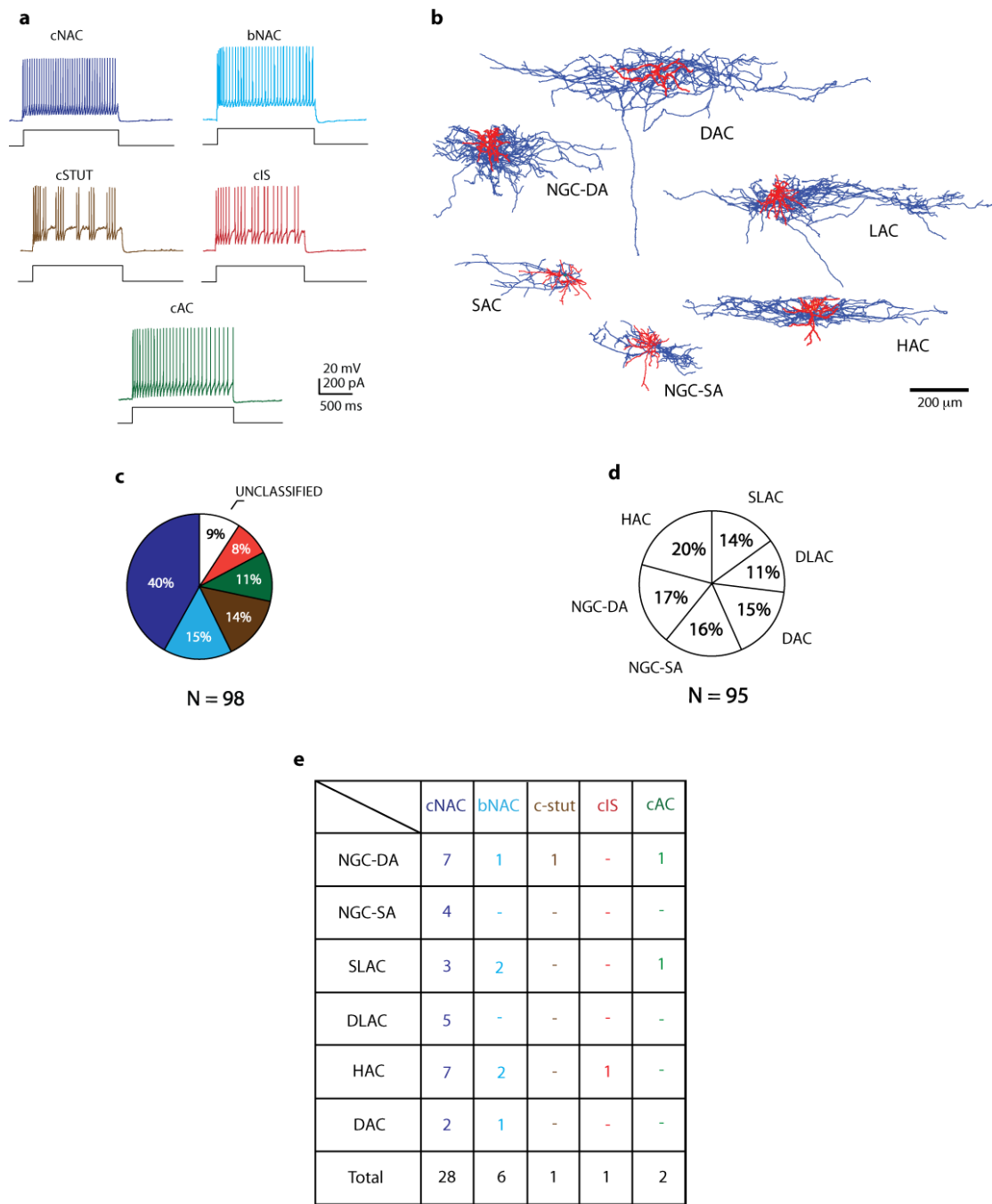


Figure 16

**Figure 16** Morpho-electrical types in L1 showing (a) firing types (b) subjective morphological classes (c) and (d) cell distributions, and (e) a numbers of cells belonging to each subtype.

## **Chapter 5 Discussion and Conclusions**

In this thesis, we characterized the single cell and microcircuit properties of the somatosensory neocortical L1 of juvenile rat, using standardised protocols for single and multi-electrode patch clamp electrophysiology, biocytin labelling and immunohistochemistry and introducing reproducible methods for the classification of electrophysiological behaviour and neuron morphologies. We identified six morphological classes of neurons, all present with approximately equal frequencies. More than 60% of these cells displayed a Non-Accommodating (NAC) pattern of firing. As already seen in previous studies, some connections among these neurons were recruited by single APs, displaying IPSP kinetics reminiscent of GABA<sub>A</sub> mediated responses. However, the majority was not activated by single APs and required high frequency trains of presynaptic APs. This is a novel finding. In some cases, the observed IPSPs were similar to GABA<sub>B</sub> mediated responses. In others they showed rise time properties characteristic of GABA<sub>A</sub> in combination with slow-decay times characteristic of GABA<sub>B</sub>. Subsequent pharmacological manipulations confirmed that GABA<sub>A</sub> and GABA<sub>B</sub> were both implicated in the IPSP kinetics.

### **Single cell properties**

#### **Electrophysiology**

In our study, as in previous work by Zhou and Hablitz, small L1 interneurons were frequently damaged or destroyed due to post-recording pipette withdrawal (Zhou and Hablitz, 1996), leading to physical damage (shrinkage and/or swelling) and loss of gigaohm seals. Despite the loss of a significant number of cells, we were nonetheless able to select a final single cell dataset of 98 cells.

Our analysis revealed that all these cells could be placed into classes based on the firing patterns described by the Petilla interneuron convention (Ascoli et al., 2008). Like the previous study (Hestrin and Armstrong, 1996), we detected non-accommodating cNAC cells (40 % of the cells in our study). Unlike these studies, we also found several other types of cell including bNAC (15%), cSTUT (14%) cAC (11%), cIR, (8%) and unclassified firing types (9%). The study did not detect the fast spiking cells reported in (Wozny and Williams, 2011). This may have been neurons begin to display FS characteristics develop relatively late in development: Wozny and Williams used older rats than those in our own study. Our failure to detect FS neurons may also be due to differences in method: we used currents of

200 pA, significantly lower than the 1 nA current used in their study. Higher currents would normally be expected to induce higher firing frequencies. However the physiological relevance of observation made under these conditions is questionable.

Similar considerations apply to the Late and Non Late spiking cells, reported by Chu et al., (Chu et al., 2003). As reported earlier, our work used a standardized current injection protocol, in which currents were scaled to produce a regulated firing frequency. This means we do not have to rely on the firing threshold, which is known to be highly variable. Chu et al, by contrast, do not attempt to maintain such a standard. It is possible, therefore, that the different spiking behaviours they observe could be the result of uncontrolled changes in threshold values. During our own experiments, we sometimes observed apparently random changes from late to non-late spiking behaviour and vice versa (data not shown). This supports the idea that early and late spiking behaviour is not sufficiently stable to be used as a criterion for electrophysiological classification of neuron types.

We believe that the methods we have applied in L1 are suitable for use with other cell populations, for example in other layers and/or areas of the cortex and in other species. In particular, we believe it is especially important to focus on firing patterns since it makes it possible to compare data for a specific population of interneurons with data for other populations as classified by the Petilla Convention (Ascoli et al., 2008).

Although the distinctions between different firing patterns were relatively clear, we are aware that our current classification is not definitive. However, these distinctions, on their own are not enough to detect the way individual ion channels affect the electrophysiological behaviour of the cell. This is a theme for future research that will probably require the development of new protocols.

## **Morphology**

In our classification of L1 morphologies we developed an initial subjective classification, and subsequently refined it using objective methods. This approach allowed us to identify six distinct morphological groups, a finer classification scheme than those developed by other authors, who reported between 2 and 4 groups.

Our classification final scheme includes three morphological types (NGCs, HACs and DACs) previously identified by Hestrin and Armstrong (Hestrin and Armstrong, 1996). Unlike these authors, however, we split the NGCs into two (NGC-SA, NGC-DA) and add two completely new types (SAC and LAC)

Like our electrophysiological classification, the methods we have used in this study are fully standardized and lend themselves to work in other layers, brain areas and species. Our objective analysis of cell types use custom written Python and MATLAB codes and are fully reproducible.

This having been said, we recognize that some aspects of our current classifier are stronger than others. In particular, there is a very clear distinction between HAC, DAC and the neurons not belonging to these types. However, the differences that distinguish NGC-SA, NGC-DA, SAC and LAC are relatively subtle and the functional relevance is an open question. It is possible that a rich classification of morphologies combined with electrophysiological data could provide a useful, multidimensional classification of electro-morphological types, as proposed by Toledo-Rodriguez (Toledo-Rodriguez et al., 2004). However, in our own study, the number of neurons with good quality electrophysiological and morphological data was too small to confirm this possibility.

### **Circuit Properties**

To our knowledge, there has only been one previous study (Chu et al., 2003) of the circuit properties of these L1 interneurons.

One of our main findings is the discovery of slow transient GABA<sub>A+B</sub> mediated IPSPs between neocortical L1 cells. This matches similar phenomena previously observed in the ferret thalamocortical loop (Kim et al., 1997), in rat neocortical layer 5 and the CA1 region of hippocampus (Thomson and Destexhe, 1999) and in connections between cortical interneurons and pyramidal cells in other layers (Chu and Hablitz, 2003; Pérez-García et al., 2006; Suzuki and Bekkers, 2010a, 2010b; Tamas et al., 2003).

A majority of these slow inhibitory connections required a 40 Hz spike train to produce a postsynaptic response. To our knowledge, no other study has documented this kind of post-synaptic GABA<sub>B</sub> response between L1 cells. Rise times varied between 5 ms and 379 ms. Response amplitudes decayed rapidly with increasing number of repetitions. We hypothesized that the decrease was due to the dilution of intracellular contents with the ICS, leading to the depletion of secondary messenger molecules such as cAMP (cyclic adenosine monophosphate). This interpretation is supported by the rapid decline in the amplitude of the IPSPs observed during repeated stimulation – exactly what we would expect with depletion of secondary messenger molecules. Perforated patch clamp experiments – which conserve the intra-cellular environment - showed no comparable decay. This is confirmatory evidence for our hypothesis.

These observations can be explained in terms of a dynamic molecular model of the binding of GABA to its receptors proposed by (Destexhe and Sejnowski, 1995). In this model, as in our own observations, IPSP responses have a slow sigmoidal rising phase and a multi-exponential decay. The authors explain this delay by the density of co-releasing terminals and the number and frequency of pre-synaptic action potentials. The model IPSPs also display a 10 - 20 ms onset delay, similar to the delay observed in our own experiments. Destexhe and Sejnowski explain this second delay by the time necessary for multiple G protein binding sites to cooperatively bind G proteins. (Destexhe and Sejnowski, 1995).

## **Conclusions**

In the study presented here, we set out to identify and characterize the components and connectivity of neocortical L1 in the somatosensory cortex of juvenile rat. We believe that we have accomplished this goal. Our results include the identification and classification of the morphologies and electrical behaviour of L1 neurons, the quantification of the presence of different morphoelectrical types, the characterization of intra-laminar connectivity, and the identification of a new kind inhibitory connection between L1 interneurons mediated by a combination of GABA<sub>A</sub> and GABA<sub>B</sub> receptors.

As far as concerns methods, we have conducted all our studies on the somatosensory cortex of rat at P13-P16. In the future, this will make it possible to connect our results to results from other groups in our lab and the Blue Brain Project, which are studying other aspects of the same area (different cortical layers, different cell populations, different levels of organization). Particularly important, in this setting, has been the development of standardised, highly reproducible methods using standard protocols and codes for the objective classification of cell firing patterns and of cell morphology,

Obviously many issues remain open. In particular, we still do not have a clear picture of the connections between L1 and other layers and of their development in older rats. Similarly, the data we have gathered is not yet sufficient to elucidate the putative role of L1 neurons in the modulation of the activity of L5PC apical dendrites or to form a detailed picture of gene expression within the layer. Nonetheless, we have explored a broad range of methods (techniques for the objective classification of cells, two-photon microscopy to study the effect of L1 stimulation on the activity of L5PC apical dendrites, isolation techniques for single cell transcriptomics). We are confident that these methods will make a valuable contribution to future studies.



## Appendix

This appendix describes three sets of additional experiments conducted during the preparation of this thesis, whose results, while not conclusive, can help to guide the design of future experiments, exploring similar scientific questions.

The first set of experiments used cytoplasmic aspirations from single cells followed by real time qPCR to study gene expression patterns in single L1 neurons. The second set studied the connectivity of L1 with PCs in L2/3 and L5. The third and final set used patch clamping and 2 photon assisted calcium imaging to investigate how apical dendritic activity in L5PCs, was affected by simultaneous stimulation of single L1 interneurons.

### Single cell transcriptomics

mRNA levels play an important role in regulating cell development and activity and may provide important predictive information about the cell's electrical behaviour and morphology. To date, however, there have been very few studies of mRNA expression in L1 cells. As with in vitro and slice studies in general, the main challenge is to achieve resolution at the single cell level.

As a method, we chose cytoplasmic aspiration followed by single cell qPCR. Assay primers were selected after careful cross checking with laboratory data on expression patterns for cortical interneurons (Toledo-Rodriguez et al., 2004) and data from the Allen Brain Atlas (<http://www.brain-map.org/>). To facilitate initial standardization experiments, we began with a small number of primers (**See table in Materials and Methods**). Statistical analyses were performed according to the methods and statistical tests cited by Zucker et al., (Zucker et al., 2005).

### Results

The threshold cycle value (Ct) for each primer indicates the PCR cycle at which the amplification of the target gene is in the mid-log phase. Lower values of Ct indicate an abundance of the target gene, and thus, ease of amplification. Higher values, conversely, denote a paucity of target gene transcripts.

V-values were calculated using beta actin as the housekeeping gene, as per the methods given in the study by Zucker et al., (Zucker et al., 2005). Ct values for beta actin were fairly constant across cells ( $Ct = 23.78 \pm 3.6$ ). To select cells for further analysis, we tested for the presence of glutamic acid decarboxylase (GAD67), a gene that codes for the

enzyme necessary for the production of GABA in the somata of interneurons. Much like beta actin, levels of GAD67 ( $Ct = 23.73 \pm 3.51$ ) were relatively constant across cells. Cells that failed to express beta actin or GAD67 were not considered in the subsequent analyses.

Apart from GAD67, the most frequently expressed gene was Reelin (35/36 cells positive;  $v$ -value 0.005.). Two other frequently expressed genes were Calretinin (Calb2) (51/69 cells positive,  $v$  value 0.15) and NPY (20/33 cells positive,  $v$  value 0.21).

The most rarely detected gene was Calbindin (Calb1) (positive expression in 7/69 cells) with a mean  $v$ -value of 0.027. The next rarest gene was GAD65, detected in 35/69 cells with a mean  $v$ -value of 1.13.

Most of the genes showed fluctuating  $v$ -values across cells, making it difficult to derive reliable quantitative estimates of expression levels. We thus interpret our results as binary indicators of the expression of specific genes.

S.no	Gene	Average $v$ -value	Number of cells	Expression (%)
1	GAD67	13.02	69	100
2	Calb1	0.027	7 (/69)	10.15
3	Calb2	0.15	51 (/69)	73.91
4	GAD65	1.13	35 (/69)	50.72
5	NPY	0.21	20 (/33)	60.6
6	Reelin	0.005	35 (/36)	97.23
7	POMC	0	0	0
8	Parvalbumin	0	0	0

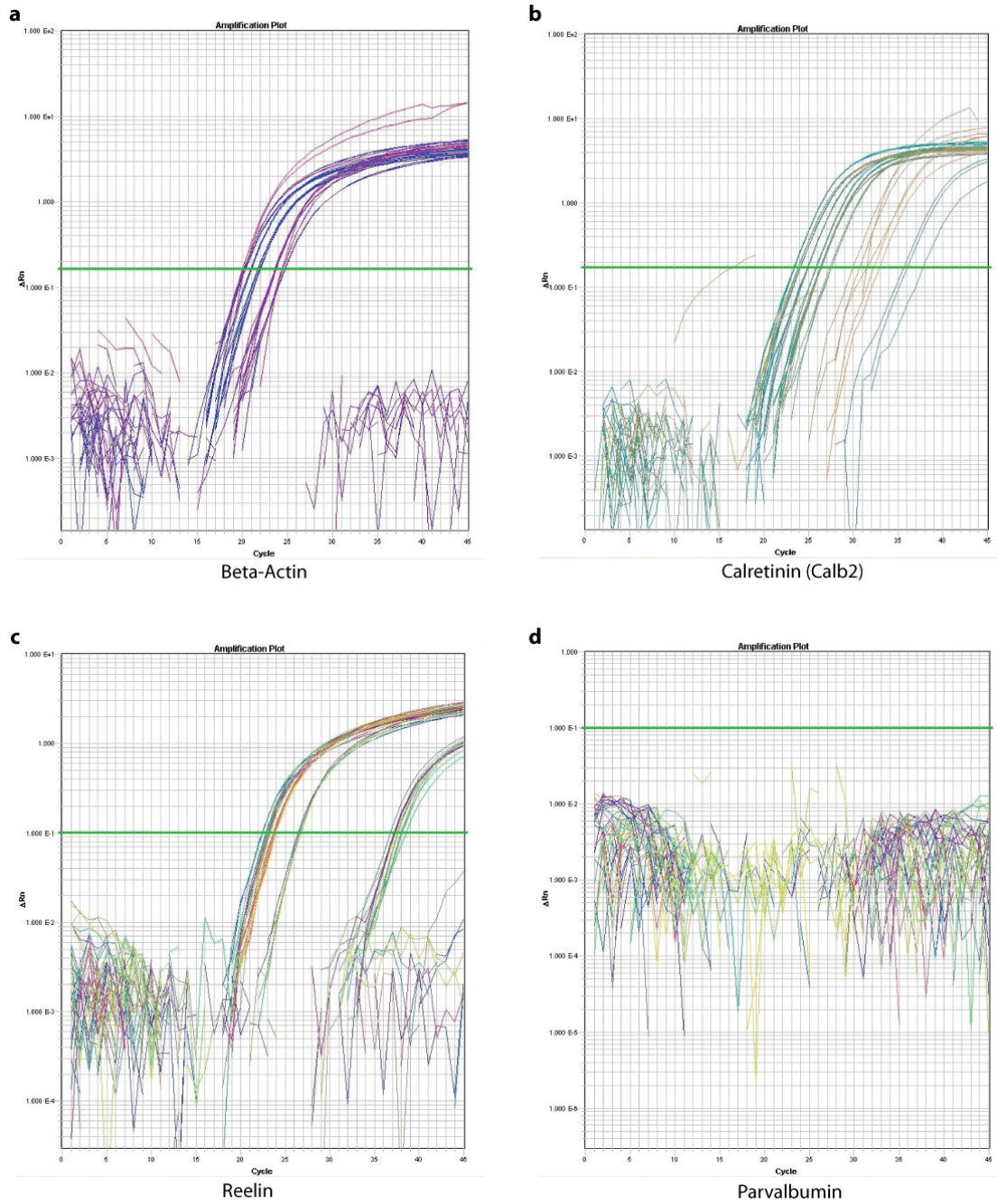


Figure 17

**Figure 17** Amplification curves for a small set of genes in the aspirated cytoplasm of two groups of L1 cells (a) shows  $\beta$ -Actin, used as a housekeeping gene (b) shows Calretinin (c) shows Reelin and (d) shows Parvalbumin which did not show any amplification in the sets of tested L1 cells.

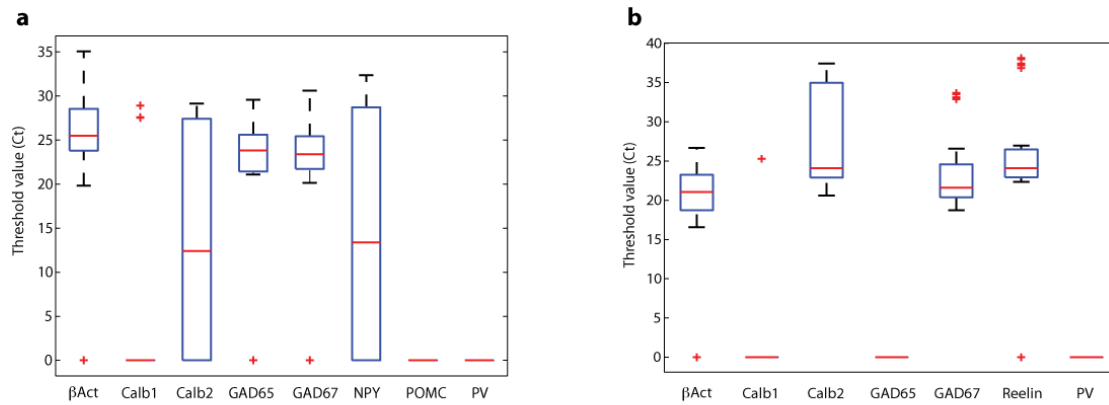


Figure 18

**Figure 18** Threshold (Ct) values for the genes tested shown in two different groups of L1 cells (a) and (b) Parvalbumin was not expressed in L1 cells along with some outlier values for Calbindin (Calb1) expression

### Expression patterns in L1

As reported earlier, our study of gene expression patterns in L1 produced extremely variable data, which was difficult to interpret. To facilitate the standardisation of protocols, we restricted our testing to a small set of genes, namely the interneuron genes listed in Toledo-Rodriguez et al., (Toledo-Rodriguez et al., 2004) and additional genes identified in the Allen Brain Atlas (<http://www.brain-map.org/>). We believe that our data can provide useful hints for the identification of markers for L1 cells and the planning of future experiments studying laminar gene expression patterns.

Our results confirmed the presence of GAD67 in these cells and thus, that L1 cells are indeed all interneurons. The expression levels for Calb1, Calb2 and PV were highly variable and did not correspond to any expression pattern previously reported for other interneurons. A high frequency of Reelin expression provided supporting evidence for the vital role of L1 cells in lamination during development.

### **Cross-layer connectivity**

The majority of information on inter-laminar connectivity comes from patch clamping pairs of cells across layers. A review article by Thomson and Lamy (Thomson and Lamy, 2007) succinctly summarises the probabilities and connection types for many cell types across all layers, except layer 1. In this study, we attempted to partially fill this gap, calculating connection probabilities and identifying the types of synapse involved. To this end, we performed 103 patch clamp experiments. In each experiment we patched two cells each in L1, L2/3 and L5 of the same cortical column and tested for connections. Overall we tested 544 cells and 1086 possible connections.

### **Results**

Our experiments detected just eight connected pairs of L1 and L2/3 cells (connection probability = 0.025 %, 320 pairs tested) and three connections between L1 cells and L5 pyramidal cells (connection probability = 0.009 %, 322 pairs tested).

IPSPs for L1 to L2/3 connections displayed slow inhibition - similar to the GABA<sub>B</sub> mediated responses observed in many connections between L1 cells (**Fig 19a**). Out of three L1 to L5 connections, one displayed slow rise and decay times (**Fig 19c**) whereas the other two showed faster rise and decay times (**Fig 19b**). These responses were abolished by perfusion of Gabazine but failed to return to normal after washout of the drug.

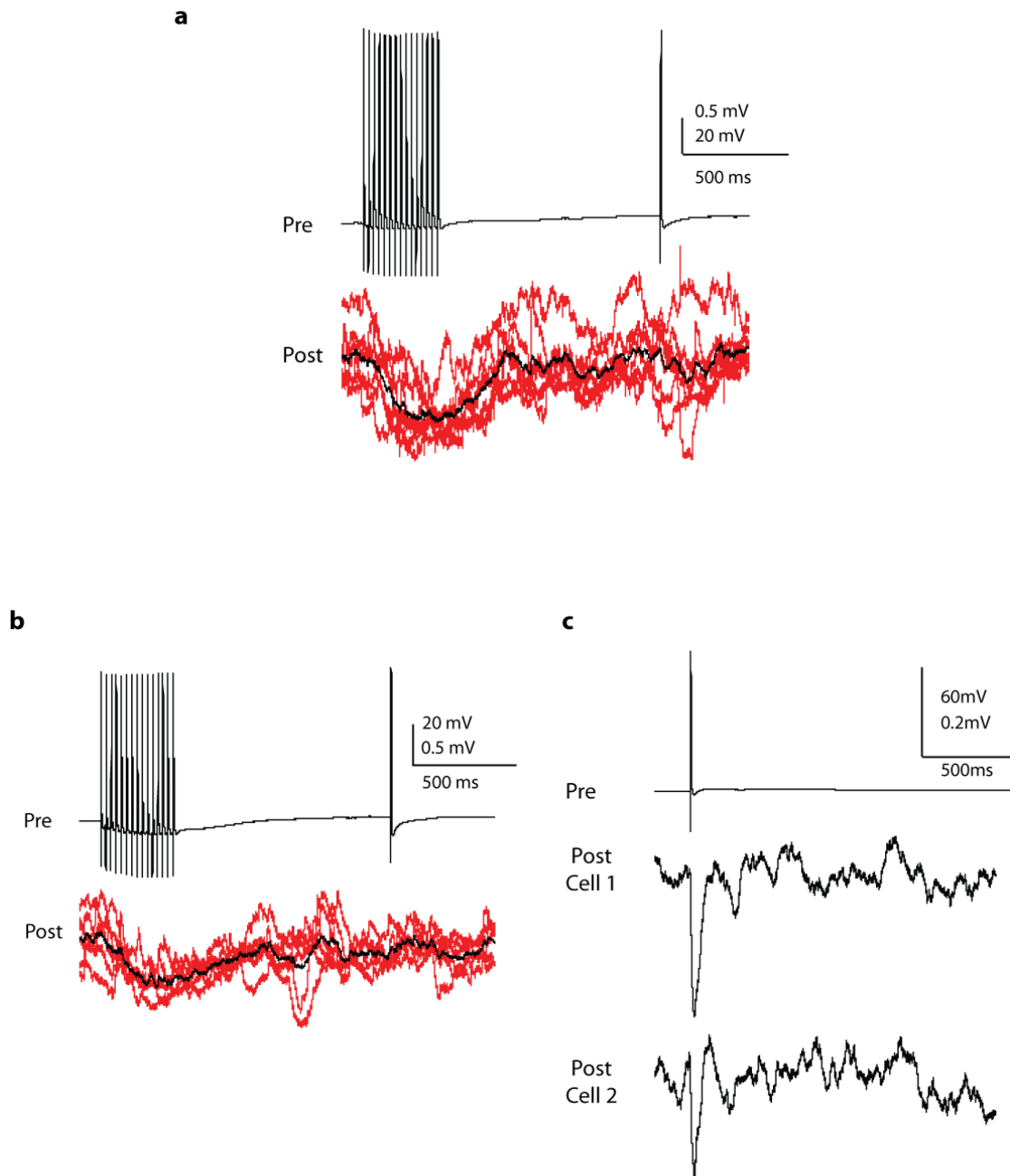


Figure 19

**Figure 19** (a) Connection between L1 cell and a L2/3 pyramidal cell. (b) and (c) connections between L1 and L5 pyramidal cells. (b) typical GABA<sub>B</sub> mediated connection with slow rise and decay times, (c) fast GABA<sub>A</sub> type IPSPs. All cells were held at -57 mV.

### **L1 and trans-laminar circuits**

Our third study investigated the probability of connections between L1 cells in general and L5 PCs, showing that the connection probability was extremely low: 0.009% (3/322). This result contrasts with the findings of a recent study (Jiang et al., 2013) published after the completion of our own work. The authors classified L1 interneurons into just two groups (SBC and ENG C), based solely on their morphological characteristics. They then measured pairwise connection probabilities for different types of cell reporting the following values: ENG Cs to L5PCs: 18.1%, SBC to L2/3 bipolar cells (BPC) 27.9%; ENG C to NGC; 42.6%). Given that we did not probe for L2/3 interneurons we cannot comment on the reported connection probabilities. Readers will however, that the authors' reported probability of connections from ENG Cs to L5PCs (18.1%) is much high than the result from our study. Given that the type and strength of connectivity between different cell populations is known to vary across development, we conjecture that the disparity in values may be related to the age of our experimental animals.

## Calcium imaging of L5PC dendrites with single cell L1 stimulation

Action potentials generated in the axon initial segment of a pyramidal neuron propagate back through the dendritic tree in a complex way that is influenced by a variety of factors. When dendritic activity coincides with a back-propagating action potential it causes calcium ion accumulation in the dendrites. Imaging of these changes in calcium concentration can detect differences in dendritic activity in L5 neurons associated with stimulation of a patched L1 neuron.

To detect these small events, we performed experiments involving a total of 7 dendritic fragments and 20 L5PCs. In each individual experiment, we patched two pyramidal cells, filled them with a calcium sensitive dye (Oregon Green BAPTA - OGB), and imaged the change in calcium concentration at the dendrites with a 2-photon microscope. Simultaneously, we patched a single L1 cell, directly above the pair of L5PCs and filled it with Alexa 594 dye, making it possible to visualise the extent of the dendrites and axons.

## Results

Single action potentials in the L5PC did not evoke a detectable calcium response in the apical dendrites. We therefore performed additional experiments to determine the number of spikes needed to elicit a reliable response. The minimal stimulus that elicited a reliable response was a pulse of 0.06 s duration with 3 spikes.

Responses to L1 stimuli were measured at 1500, 1000 and 500 ms before and after L5PC stimulation. **Fig 20a** shows the schematic of the experiment and **Fig 20b** shows the stimulation pattern.

The experiments showed no measurable effect of stimulation of L1 cells on L5 dendritic activity. The mean amplitude of the normalized  $\Delta F/F$  values ( $0.844 \pm 0.02$  (mean  $\pm$  S.D)) did not show any significant change between time points and across experiments (**Fig 20c**). **Fig 20d** shows the negligible change in decay kinetics of the calcium response across stimulation times and dendrites.



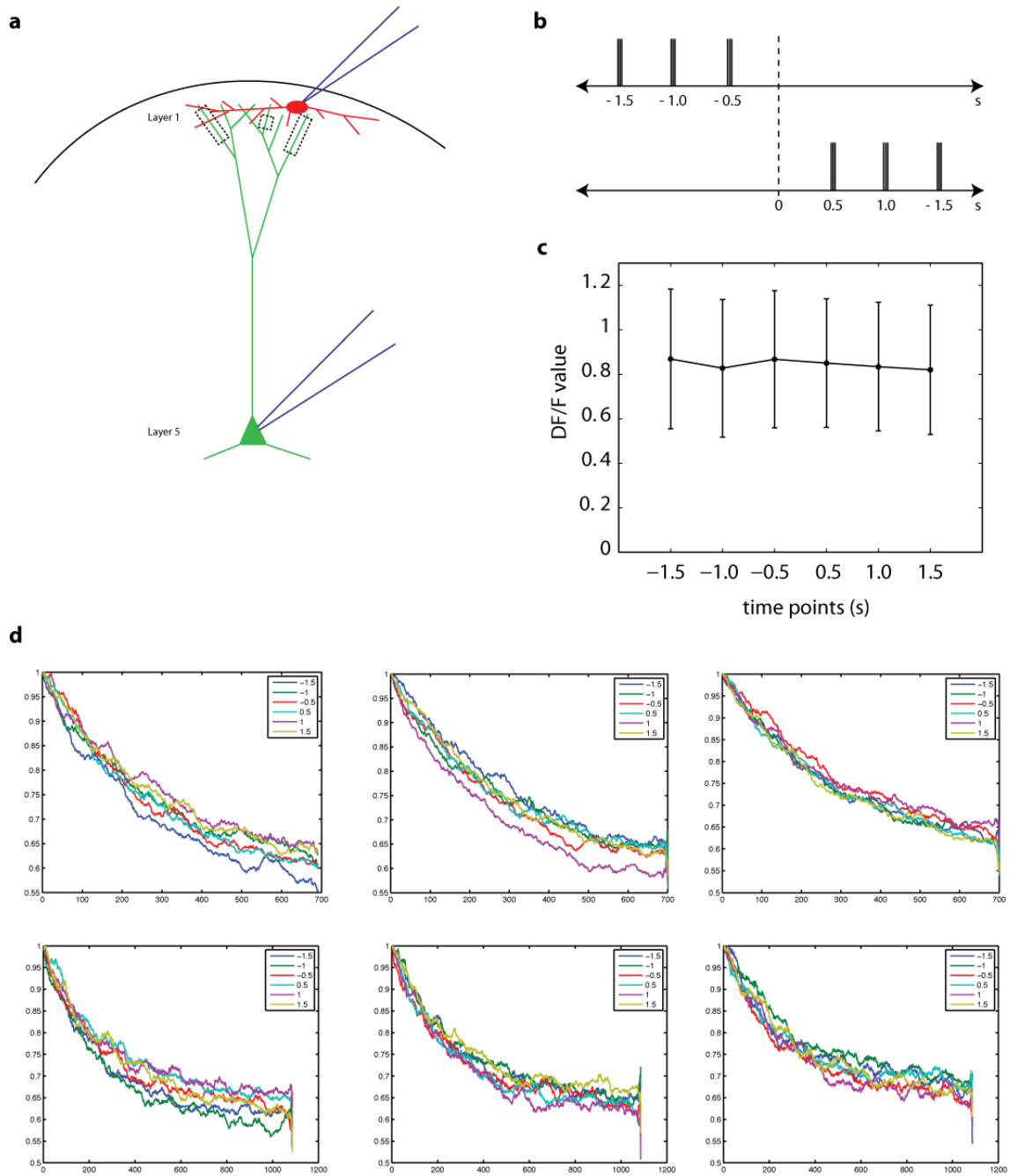


Figure 20

**Figure 20** (a) A L1 neuron filled with Alexa 594 and L5PC with OGB. (b) The protocol used to stimulate L5PCs and L1 neurons.  $t = 0$  seconds indicates the time of stimulation of the L1 neuron. The L5PC was stimulated at various time points (1.5s, 1.0s and 0.5s) before and after  $t = 0$  seconds. (c) average values of  $\Delta F/F$  imaged and calculated at the different dendritic sites. The large error bars negate the evidence of any effect of L1 single neuron stimulation on L5PC apical dendritic activation (d) three repetitions of calcium activity recorded from two different dendritic segments. The decays at the six different time points are colour coded. We saw no change in the decay time kinetics across dendritic segments.

### **Interaction with apical pyramidal dendrites**

Calcium-mediated APs, generated locally at the L5PC apical dendrites, projecting to L1, couple synaptic inputs from different cortical layers and interact with back-propagated AP from the soma, supporting the detection of coincident signals arriving within a given time window (Larkum et al., 1999, 2001; Schaefer et al., 2003; Spruston, 2008). Given the position of L1 in the neocortex, it is possible that GABAergic L1 cells modulate this activity. GABA<sub>B</sub> receptors on the membrane of these apical extremities (Kulik et al., 2003; López-Bendito et al., 2002), are known to directly block the dendritic Ca<sup>2+</sup> channels responsible for Ca<sup>2+</sup>-AP (Pérez-García et al., 2006), making them less sensitive to incoming stimuli including thalamo-cortical inputs and back-propagating action potentials.

To investigate this possibility, we use a two-photon microscope to image dye-filled apical dendrites of L5PCs while simultaneously stimulating single L1 cells. However, we were unable to observe any change in the amplitudes and decay time kinetics of the calcium transients. It is known that the density of calcium and sodium channels at the apical dendritic tufts is suboptimal in young rats such as those we used in our study (P13 to P16) (Hamill et al., 1991; Kang et al., 1996). It is likely, therefore, that the calcium transients elicited by stimulation will be weak.

We also filled the L1 neurons for the same period as the L5PCs. Thus, it is very likely that the dilution of the secondary messenger molecules, have led to a much weaker release of GABA. It is also possible that the stimulation of single L1 cells does not release enough GABA in the vicinity of the GABA<sub>B</sub> receptors to elicit detectable calcium transients (Destexhe and Sejnowski, 1995). We could not test this since we did not use the 40Hz 15 spike train that we used to test connections between L1 cells. Thus, even though our experiments show no evidence of the effect, it would be premature to conclude that there is no effect. Further investigations could use channelrhodopsin experiments or glutamate uncaging to ensure precise and reliable activation of the desired synapses.

## References

- Aguilo, A., Schwartz, T., Kumar, V., Peterlin, Z., Tsiola, A., Soriano, E., and Yuste, R. (1999). Involvement of Cajal-Retzius Neurons in Spontaneous Correlated Activity of Embryonic and Postnatal Layer 1 from Wild-Type and Reeler Mice. *Journal of Neuroscience* *19*, 10856.
- Ascoli, G.A., Alonso-Nanclares, L., Anderson, S.A., Barrionuevo, G., Benavides-Piccione, R., Burkhalter, A., Buzsáki, G., Cauli, B., Defelipe, J., Fairén, A., et al. (2008). Petilla terminology: nomenclature of features of GABAergic interneurons of the cerebral cortex. *Nat Rev Neurosci* *9*, 557–568.
- Bradford, R., Parnavelas, J., and Lieberman, A. (1977). Neurons in layer I of the developing occipital cortex of the rat. *The Journal of Comparative Neurology* *176*, 121–132.
- Cajal, S.R. y (1995). *Histology of the Nervous System of Man and Vertebrates (History of Neuroscience, No 6)* (Oxford University Press, USA).
- Cauli, B., Audinat, E., Lambolez, B., Angulo, M., Ropert, N., Tsuzuki, K., Hestrin, S., and Rossier, J. (1997). Molecular and Physiological Diversity of Cortical Nonpyramidal Cells. *Journal of Neuroscience* *17*, 3894.
- Cauller, L. (1995). Layer I of primary sensory neocortex: where top-down converges upon bottom-up. *Behav Brain Res* *71*, 163–170.
- Chu, Z., and Hablitz, J.J. (2003). GABA(B) receptor-mediated heterosynaptic depression of excitatory synaptic transmission in rat frontal neocortex. *Brain Res* *959*, 39–49.
- Chu, Z., Galarreta, M., and Hestrin, S. (2003). Synaptic interactions of late-spiking neocortical neurons in layer 1. *J Neurosci* *23*, 96–102.
- Destexhe, A., and Sejnowski, T.J. (1995). G protein activation kinetics and spillover of gamma-aminobutyric acid may account for differences between inhibitory responses in the hippocampus and thalamus. *Proceedings of the National Academy of Sciences of the United States of America* *92*, 9515–9519.
- Fulton, J.F. (1949). *Physiology of the nervous system* (Oxford University Press).
- Gabbott, P.L., and Somogyi, P. (1986). Quantitative distribution of GABA-immunoreactive neurons in the visual cortex (area 17) of the cat. *Exp Brain Res* *61*, 323–331.
- Gentet, L.J., Avermann, M., Matyas, F., Staiger, J.F., and Petersen, C.C.H. (2010). Membrane Potential Dynamics of GABAergic Neurons in the Barrel Cortex of Behaving Mice. *Neuron* *65*, 422–435.
- Hamill, O.P., Huguenard, J.R., and Prince, D.A. (1991). Patch-clamp studies of voltage-gated currents in identified neurons of the rat cerebral cortex. *Cereb. Cortex* *1*, 48–61.

Hernando, J., Schurmann, F., Markram, H., and Anasagasti, Hm. (2008). RTNeuron, an Application for Interactive Visualization of Detailed Cortical Column Simulations. *Jornadas de Paralelismo XVIII*.

Hestrin, S., and Armstrong, W.E. (1996). Morphology and physiology of cortical neurons in layer I. *J Neurosci* 16, 5290–5300.

Jiang, X., Wang, G., Lee, A.J., Stornetta, R.L., and Zhu, J.J. (2013). The organization of two new cortical interneuronal circuits. *Nature Neuroscience* 16, 210–218.

Jolliffe, I.T. (2002). *Principal Component Analysis* (Springer).

Kaas, J.H. (2009). *Evolutionary Neuroscience* (Academic Press).

Kandel, E.R., Schwartz, J.H., Jessell, T.M., Siegelbaum, S.A., and Hudspeth, A.J. (2012). *Principles of Neural Science* (New York: The McGraw Hill companies).

Kang, J., Huguenard, J.R., and Prince, D.A. (1996). Development of BK channels in neocortical pyramidal neurons. *J Neurophysiol* 76, 188–198.

Kawaguchi, Y. (1995). Physiological subgroups of nonpyramidal cells with specific morphological characteristics in layer II/III of rat frontal cortex. *J. Neurosci.* 15, 2638–2655.

Kawaguchi, Y., and Kondo, S. (2002). Parvalbumin, somatostatin and cholecystokinin as chemical markers for specific GABAergic interneuron types in the rat frontal cortex. *J. Neurocytol.* 31, 277–287.

Kawaguchi, Y., and Kubota, Y. (1997). GABAergic cell subtypes and their synaptic connections in rat frontal cortex. *Cereb. Cortex* 7, 476–486.

Kim, U., Sanchez-Vives, M.V., and McCormick, D.A. (1997). Functional dynamics of GABAergic inhibition in the thalamus. *Science* 278, 130–134.

Kisvárdy, Z.F., Gulyas, A., Beroukas, D., North, J.B., Chubb, I.W., and Somogyi, P. (1990). Synapses, axonal and dendritic patterns of GABA-immunoreactive neurons in human cerebral cortex. *Brain* 113 ( Pt 3), 793–812.

Krzanowski, W.J. (2000). *Principles of Multivariate Analysis: A User's Perspective* (Oxford University Press, USA).

Kubota, Y., and Kawaguchi, Y. (1994). Three classes of GABAergic interneurons in neocortex and neostriatum. *Jpn. J. Physiol.* 44 Suppl 2, S145–148.

Kulik, Á., Vida, I., Luján, R., Haas, C.A., López-Bendito, G., Shigemoto, R., and Frotscher, M. (2003). Subcellular Localization of Metabotropic GABAB Receptor Subunits GABAB1a/b and GABAB2 in the Rat Hippocampus. *J. Neurosci.* 23, 11026–11035.

Lacor, P.N., Grayson, D.R., Auta, J., Sugaya, I., Costa, E., and Guidotti, A. (2000). Reelin secretion from glutamatergic neurons in culture is independent from neurotransmitter regulation. *Proc Natl Acad Sci U S A* 97, 3556–3561.

Larkum, M.E., Zhu, J.J., and Sakmann, B. (1999). A new cellular mechanism for coupling inputs arriving at different cortical layers. *Nature* 398, 338–341.

Larkum, M.E., Zhu, J.J., and Sakmann, B. (2001). Dendritic mechanisms underlying the coupling of the dendritic with the axonal action potential initiation zone of adult rat layer 5 pyramidal neurons. *The Journal of Physiology* 533, 447–466.

Letzkus, J.J., Wolff, S.B.E., Meyer, E.M.M., Tovote, P., Courtin, J., Herry, C., and Lüthi, A. (2011). A disinhibitory microcircuit for associative fear learning in the auditory cortex. *Nature* 480, 331–335.

Lima, S.Q., and Miesenböck, G. (2005). Remote control of behavior through genetically targeted photostimulation of neurons. *Cell* 121, 141–152.

López-Bendito, G., Shigemoto, R., Kulik, A., Paulsen, O., Fairén, A., and Luján, R. (2002). Expression and distribution of metabotropic GABA receptor subtypes GABABR1 and GABABR2 during rat neocortical development. *European Journal of Neuroscience* 15, 1766–1778.

Markram, H., Lübke, J., Frotscher, M., Roth, A., and Sakmann, B. (1997). Physiology and anatomy of synaptic connections between thick tufted pyramidal neurones in the developing rat neocortex. *J. Physiol. (Lond.)* 500 ( Pt 2), 409–440.

Meyer, G., and Goffinet, A.M. (1998). Prenatal development of reelin-immunoreactive neurons in the human neocortex. *J. Comp. Neurol.* 397, 29–40.

Meyer, G., Goffinet, A.M., and Fairén, A. (1999). What is a Cajal-Retzius cell? A reassessment of a classical cell type based on recent observations in the developing neocortex. *Cereb. Cortex* 9, 765–775.

Mountcastle, V.B. (1957). Modality and Topographic Properties of Single Neurons of Cat's Somatic Sensory Cortex. *J Neurophysiol* 20, 408–434.

Neher, E., Sakmann, B., and Steinbach, J.H. (1978). The extracellular patch clamp: a method for resolving currents through individual open channels in biological membranes. *Pflügers Arch.* 375, 219–228.

Oberlaender, M., Boudewijns, Z.S.R.M., Kleele, T., Mansvelder, H.D., Sakmann, B., and Kock, C.P.J. de (2011). Three-dimensional axon morphologies of individual layer 5 neurons indicate cell type-specific intracortical pathways for whisker motion and touch. *Proceedings of the National Academy of Sciences of the United States of America* 108, 4188–4193.

Oda, S., Kishi, K., Yang, J., Chen, S., Yokofujita, J., Igarashi, H., Tanihata, S., and Kuroda, M. (2004). Thalamocortical projection from the ventral posteromedial nucleus sends its collaterals to layer I of the primary somatosensory cortex in rat. *Neurosci Lett* 367, 394–398.

Palmer, L.M., Schulz, J.M., Murphy, S.C., Ledergerber, D., Murayama, M., and Larkum, M.E. (2012). The cellular basis of GABA(B)-mediated interhemispheric inhibition. *Science* 335, 989–993.

- Parker, G.H. (2012). *The Elementary Nervous System* (Hard Press).
- Pedregosa, F. (2011). Scikit-learn: Machine Learning in {P}ython. *Journal of Machine Learning Research* 12, 2825 – 2830.
- Pérez-Garci, E., Gassmann, M., Bettler, B., and Larkum, M.E. (2006). The GABAB1b isoform mediates long-lasting inhibition of dendritic Ca<sup>2+</sup> spikes in layer 5 somatosensory pyramidal neurons. *Neuron* 50, 603–616.
- Perin, R., Berger, T.K., and Markram, H. (2011). A synaptic organizing principle for cortical neuronal groups. *Proc. Natl. Acad. Sci. U.S.A.* 108, 5419–5424.
- Peters, A., and Jones, E.G. (1984). *Cerebral cortex* (New York: Plenum Press).
- Peters, A., and Jones, E.G. (1985). *Cerebral Cortex: Visual Cortex* (Plenum Press).
- Portera-Cailliau, C., Weimer, R.M., Paola, V.D., Caroni, P., and Svoboda, K. (2005). Diverse modes of axon elaboration in the developing neocortex. *PLoS Biol* 3, 272.
- Ribak, C.E. (1978). Aspinous and sparsely-spinous stellate neurons in the visual cortex of rats contain glutamic acid decarboxylase. *J. Neurocytol.* 7, 461–478.
- Ribak, C.E., Vaughn, J.E., and Roberts, E. (1979). The GABA neurons and their axon terminals in rat corpus striatum as demonstrated by GAD immunocytochemistry. *J. Comp. Neurol.* 187, 261–283.
- Rubio-Garrido, P., Pérez-de-Manzo, F., Porrero, C., Galazo, M.J., and Clascá, F. (2009). Thalamic Input to Distal Apical Dendrites in Neocortical Layer 1 Is Massive and Highly Convergent. *Cereb. Cortex* 19, 2380–2395.
- Sakmann, B., and Neher, E. (2009). *Single-Channel Recording* (Springer).
- Schaefer, A.T., Larkum, M.E., Sakmann, B., and Roth, A. (2003). Coincidence detection in pyramidal neurons is tuned by their dendritic branching pattern. *Journal of Neurophysiology* 89, 3143–3154.
- Spruston, N. (2008). Pyramidal neurons: dendritic structure and synaptic integration. *Nat Rev Neurosci* 9, 206–221.
- Steriade, M. (2001). *The Intact and Sliced Brain* (Bradford).
- Stuart, G.J., Dodt, H.U., and Sakmann, B. (1993). Patch-clamp recordings from the soma and dendrites of neurons in brain slices using infrared video microscopy. *Pflugers Arch.* 423, 511–518.
- Suzuki, N., and Bekkers, J.M. (2010a). Distinctive Classes of GABAergic Interneurons Provide Layer-Specific Phasic Inhibition in the Anterior Piriform Cortex. *Cereb Cortex*.
- Suzuki, N., and Bekkers, J.M. (2010b). Inhibitory neurons in the anterior piriform cortex of the mouse: classification using molecular markers. *The Journal of Comparative Neurology* 518, 1670–1687.

Swisher, J.D., Gatenby, J.C., Gore, J.C., Wolfe, B.A., Moon, C.-H., Kim, S.-G., and Tong, F. (2010). Multiscale Pattern Analysis of Orientation-Selective Activity in the Primary Visual Cortex. *J. Neurosci.* *30*, 325–330.

Szabadics, J., Tamás, G., and Soltesz, I. (2007). Different transmitter transients underlie presynaptic cell type specificity of GABA<sub>A</sub>,slow and GABA<sub>A</sub>,fast. *PNAS* *104*, 14831–14836.

Tamas, G., Simon, A.L., and Szabadics, J. (2003). Identified Sources and Targets of Slow Inhibition in the Neocortex. 1902–1905.

Thomson, A.M., and Destexhe, A. (1999). Dual intracellular recordings and computational models of slow inhibitory postsynaptic potentials in rat neocortical and hippocampal slices. *Neuroscience* *92*, 1193–1215.

Thomson, A.M., and Deuchars, J. (1997). Synaptic interactions in neocortical local circuits: dual intracellular recordings in vitro. *Cereb Cortex* *7*, 510–522.

Thomson, A.M., and Lamy, C. (2007). Functional maps of neocortical local circuitry. *Frontiers in Neuroscience* *1*, 19–42.

Thomson, A.M., West, D.C., Hahn, J., and Deuchars, J. (1996). Single axon IPSPs elicited in pyramidal cells by three classes of interneurons in slices of rat neocortex. *The Journal of Physiology* *496 (Pt 1)*, 81–102.

Toledo-Rodriguez, M., Blumenfeld, B., Wu, C., Luo, J., Attali, B., Goodman, P., and Markram, H. (2004). Correlation Maps Allow Neuronal Electrical Properties to be Predicted from Single-cell Gene Expression Profiles in Rat Neocortex. *Cereb. Cortex* *14*, 1310–1327.

Toyama, K., Matsunami, K., Ono, T., and Tokashiki, S. (1974). An intracellular study of neuronal organization in the visual cortex. *Exp Brain Res* *21*, 45–66.

Wang, Y., Gupta, A., Toledo-Rodriguez, M., Wu, C.Z., and Markram, H. (2002). Anatomical, Physiological, Molecular and Circuit Properties of Nest Basket Cells in the Developing Somatosensory Cortex. 395–410.

Wang, Y., Toledo-Rodriguez, M., Gupta, A., Wu, C., Silberberg, G., Luo, J., and Markram, H. (2004). Anatomical, physiological and molecular properties of Martinotti cells in the somatosensory cortex of the juvenile rat. *The Journal of Physiology* *561*, 65–90.

Wonders, C.P., and Anderson, S.A. (2006). The origin and specification of cortical interneurons. *Nat Rev Neurosci* *7*, 687–696.

Woolsey, T.A., and Van der Loos, H. (1970). The structural organization of layer IV in the somatosensory region (S I) of mouse cerebral cortex: The description of a cortical field composed of discrete cytoarchitectonic units. *Brain Research* *17*, 205–242.

Wozny, C., and Williams, S.R. (2011). Specificity of synaptic connectivity between layer 1 inhibitory interneurons and layer 2/3 pyramidal neurons in the rat neocortex. *Cereb. Cortex* *21*, 1818–1826.

Zemelman, B.V., Lee, G.A., Ng, M., and Miesenböck, G. (2002). Selective photostimulation of genetically chARGed neurons. *Neuron* 33, 15–22.

Zhou, F.-M., and Hablitz, J.J. (1996). Morphological properties of intracellularly labeled layer I neurons in rat neocortex. *The Journal of Comparative Neurology* 376, 198–213.

Zucker, B., Luthi-Carter, R., Kama, J.A., Dunah, A.W., Stern, E.A., Fox, J.H., Standaert, D.G., Young, A.B., and Augood, S.J. (2005). Transcriptional dysregulation in striatal projection-and interneurons in a mouse model of Huntington's disease: neuronal selectivity and potential neuroprotective role of HAP1. *Human Molecular Genetics* 14, 179.



# Curriculum Vitae

# Shruti Muralidhar

Avenue de Mon Repos 4, Lausanne, 1005 Switzerland  
Phone: 0041 79 842 5989 E-Mail: [shruti.muralidhar@epfl.ch](mailto:shruti.muralidhar@epfl.ch)

Date of Birth: 10<sup>th</sup> of February 1985

## Education

- Currently pursuing a doctoral degree in Neuroscience at the Ecole Polytechnique Federale de Lausanne (EPFL), Switzerland January 2008 to present
- Masters in Neuroscience from the National Brain Research Centre (NBRC), Haryana, India August 2005 to September 2006
- Bachelors (Hon) in Biomedical Sciences from Acharya Narendra Dev College, Delhi University, India July 2002 to July 2005
- All India Senior School Certificate Examination (AISSCE) under the Central Board of Secondary Education (CBSE) from Lady Irwin School, New Delhi June 2002

## Research Experience

- **Synaptic and Cellular organisation of neocortical layer 1 in the developing rat somatosensory cortex**, PhD thesis with Prof Henry Markram at Ecole Polytechnique Federale de Lausanne, Switzerland January 2008 to present
- **Effect of stem cell injections on dorsal cervical injuries in rats**, Masters' thesis with Prof. Neeraj Jain at the National Brain Research Centre (NBRC), Haryana, India July 2006 to August 2007
- **Basic techniques in molecular biology, coding in MATLAB and immunohistochemistry** during rotations in various laboratories of the National Brain Research Centre (NBRC), Haryana, India July 2005 to May 2006
- **The effect of Octopamine on feeding behaviour of *Drosophila melanogaster***, Summer project with Prof. VijayRaghavan at the National Centre for Biological Sciences (NCBS), Bangalore, India June 2004 to July 2004

## Publications/Presentations

- Synaptic and Cellular Organisation of Neocortical layer 1 in the juvenile rat somatosensory cortex In preparation
- Poster at FENS in Barcelona, Spain July 2012
- Poster at Society for Neuroscience (SfN) in Washington DC, USA November 2011
- Poster at Society for Neuroscience (SfN) in Chicago, USA October 2009

# Shruti Muralidhar

Avenue de Mon Repos 4, Lausanne, 1005 Switzerland  
Phone: 0041 79 842 5989 E-Mail: [shruti.muralidhar@epfl.ch](mailto:shruti.muralidhar@epfl.ch)

Date of Birth: 10<sup>th</sup> of February 1985

## Expertise

- Patch clamp electrophysiology techniques (upto 6 cells), including basic setup of rig hardware and software
- Rodent handling and basic behavioural experimental techniques
- Molecular biology techniques including real time PCR and immunostaining

## Non-academic achievements

- One of five finalists from Suisse Romande for Famelab, an international competition in science communication for young researchers (<http://www.famelab.ch/en/content/swiss-final-2012>)

## Interests

- Science writing and communication, classical music (amateur cellist), reading fiction, computer gaming, nature hikes, swimming, basketball, quizzing.

## Languages

- Fluent (written and spoken) : English and Hindi
- Conversational : Tamil, Marathi and French